Article

A tissue-like neurotransmitter sensor for the brain and gut

https://doi.org/10.1038/s41586-022-04615-2

Received: 15 June 2020

Accepted: 4 March 2022

Published online: 1 June 2022

Check for updates

Jinxing Li[1,2,11], Yuxin Liu[3,11], Lei Yuan[4,11], Baibing Zhang[4], Estelle Spear Bishop[5], Kecheng Wang[6], Jing Tang[6], Yu-Qing Zheng[1], Wenhui Xu[6], Simiao Niu[1], Levent Beker[1], Thomas L. Li[7,8], Gan Chen[6], Modupeola Diyaolu[9], Anne-Laure Thomas[9], Vittorio Mottini[1,2], Jeffrey B.-H. Tok[1], James C. Y. Dunn[3,9], Bianxiao Cui[7], Sergiu P. Paşca[8,10], Yi Cui[6], Aida Habtezion[5], Xiaoke Chen[4]✉ & Zhenan Bao[1]✉

Neurotransmitters play essential roles in regulating neural circuit dynamics both in the central nervous system as well as at the peripheral, including the gastrointestinal tract[1–3]. Their real-time monitoring will offer critical information for understanding neural function and diagnosing disease[1–3]. However, bioelectronic tools to monitor the dynamics of neurotransmitters in vivo, especially in the enteric nervous systems, are underdeveloped. This is mainly owing to the limited availability of biosensing tools that are capable of examining soft, complex and actively moving organs. Here we introduce a tissue-mimicking, stretchable, neurochemical biological interface termed NeuroString, which is prepared by laser patterning of a metal-complexed polyimide into an interconnected graphene/nanoparticle network embedded in an elastomer. NeuroString sensors allow chronic in vivo real-time, multichannel and multiplexed monoamine sensing in the brain of behaving mouse, as well as measuring serotonin dynamics in the gut without undesired stimulations and perturbing peristaltic movements. The described elastic and conformable biosensing interface has broad potential for studying the impact of neurotransmitters on gut microbes, brain–gut communication and may ultimately be extended to biomolecular sensing in other soft organs across the body.

Soft tissues and organs in the human body are highly active biochemical systems that include biomolecules, such as neurotransmitters and hormones, precisely controlling various biological processes. Monitoring the dynamics of neurotransmitters is essential to understanding the communication between neurons and their targets, and to develop therapeutic neuromodulatory strategies[1–3]. In the central nervous system (CNS), monoamines, including dopamine (DA) and serotonin (5-HT), are involved in the regulation of cognitive processes such as emotion, arousal and memory[4,5]. Dysregulated monoamine signalling is a common feature of many psychiatric and neurological disorders, including addiction, major depressive disorder and Parkinson disease[6–8]. Outside the CNS, 5-HT in the gastrointestinal (GI) system accounts for 95% of the body's 5-HT and closely regulates gut function and microbiota, serving as an important component of the gut–brain communication system[9,10]. Therefore, there is great interest in monitoring the dynamics of monoamines in both the CNS and the GI system.

Nevertheless, the tools for studying biochemical signalling in vivo remain limited. The recent development of genetically encoded fluorescence sensors offered many advantages in terms of sensitivity, selectivity and fast dynamics[1,11,12]. Alternatively, the analytical voltammetry method offers great potential for clinical bioelectronics use, as it is universally applicable for wild-type animals without transgenic modification[13–17] and has been adopted to study the monoamine dynamics in human participants[18,19]. The recent advances of neural probes and bioelectronics have primarily focused on developing soft or miniaturized electrophysiological devices[20–25]. However, current instruments for voltammetry neurotransmitter sensing mostly rely on silica-encapsulated carbon fibre electrodes, which are rigid and brittle, and have limited tunability of sensing functions[17]. These rigid probes might lead to early device failure or severe inflammatory response, as the brain is undergoing constant motion and deformation owing to the cardiorespiratory cycles and body movements[26–28]. Similarly, the GI tract is made of a series of soft, long and twisting organs with a variety of motility patterns (peristaltic or non-peristaltic) and abundant mechanoreceptors[29,30]. Performing high-fidelity electrical or optical measurements of 5-HT dynamics in an actively moving GI tract has been a long-standing challenge[31].

Here we introduce a soft and stretchable graphene-based biosensing neural interface, termed 'NeuroString', to seamlessly interface with CNS and GI tissue, and enable real-time simultaneous monitoring

[1]Department of Chemical Engineering, Stanford University, Stanford, CA, USA. [2]Department of Biomedical Engineering and Institute for Quantitative Health Science and Engineering, Michigan State University, East Lansing, MI, USA. [3]Department of Bioengineering, Stanford University, Stanford, CA, USA. [4]Department of Biology, Stanford University, Stanford, CA, USA. [5]Division of Gastroenterology and Hepatology, Stanford University School of Medicine, Stanford, CA, USA. [6]Department of Materials Science and Engineering, Stanford University, Stanford, CA, USA. [7]Department of Chemistry, Stanford University, Stanford, CA, USA. [8]Department of Psychiatry and Behavioral Sciences, Stanford University, Stanford, CA, USA. [9]Department of Surgery/Pediatric Surgery, Stanford University, Stanford, CA, USA. [10]Stanford Brain Organogenesis, Wu Tsai Neurosciences Institute and Bio-X, Stanford University, Stanford, CA, USA. [11]These authors contributed equally: Jinxing Li, Yuxin Liu, Lei Yuan. ✉e-mail: xkchen@stanford.edu; zbao@stanford.edu

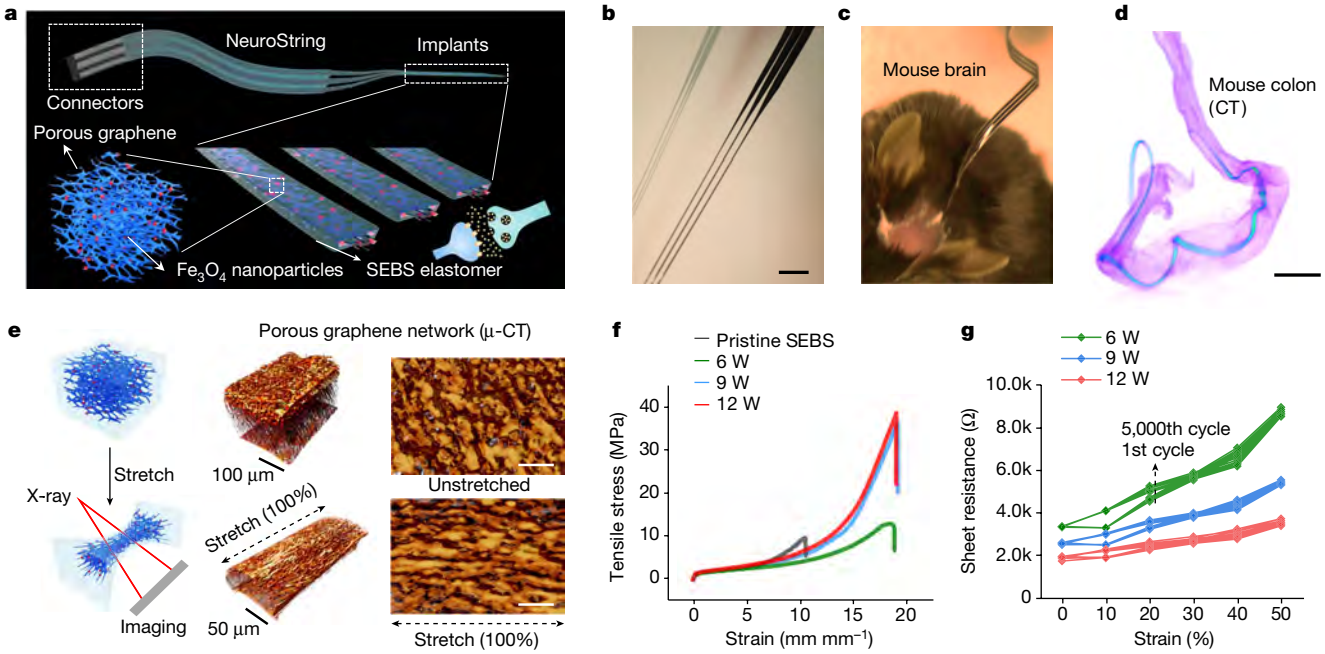

Fig. 1 | NeuroString for sensing neurotransmitters in the brain and gut. **a**, Schematic of the soft implant for sensing neurotransmitters in the brain and 3D schematic showing the composite materials made by confining nanoscale graphene/iron oxide nanoparticle networks in an elastomer (SEBS) to construct a soft, sensitive and selective neurochemical sensor. **b**, A stretched three-channel NeuroString with each channel for sensing brain neurotransmitters separately. The scale bar denotes 3 mm. **c**, NeuroString chronically implanted in a mouse. **d**, Ex vivo X-ray CT showing a gut NeuroString placed in the mouse colon. The scale bar denotes 5 mm. **e**, Left, schematic setup for in situ characterization of the graphene mesostructure under strain. Middle, X-ray tomography 3D reconstruction of the graphene–elastomer composite showing the mesostructure of the graphene nanofibre networks at 0% (upper) and 100% (bottom) strain, respectively. Right, corresponding top view of the graphene tomography. The scale bars denote 5 μm. The μ-CT scan results were repeated and reproduced three times. **f**, Tensile stress–strain behaviour of the graphene–elastomer composites prepared by different laser power. **g**, Sheet resistance of the graphene–elastomer composites prepared by different laser power under different strains and stretching cycles (strain from 0% to 50% for 5,000 cycles, data showing the sheet resistance of the 1st, 1,000th, 2,000th, 3,000th, 4,000th and 5,000th stretching cycles).

of monoamine dynamics in both tissues (Fig. 1a–d). Graphene was selected as the electrode material owing to its good biocompatibility, high super-capacitive response during fast-scan cyclic voltammetry (FSCV), known catalytic activity towards amine oxidation[32,33], as well as high mechanical compliance in bending, stretching and twisting resulting from its atomic-level thickness. However, graphene monolayer cracks at less than 5% strain[34]. We address this issue by embedding laser-induced graphene nanofibre networks, with transition metal nanoparticles decorated on the surface, into a polystyrene-*block*-poly(ethylene-*ran*-butylene)-block-polystyrene (SEBS) elastomer matrix to achieve high levels of softness and stretchability while preserving the unique electrochemical properties of the nanomaterials (Fig. 1a).

Two separate fabrication processes were developed for devices used in the CNS and the GI tract, respectively (Extended Data Fig. 1). Transition metal nanoparticles (such as Fe_3O_4 or NiO nanoparticles) are known to promote molecular absorption and electron transfer to catalytically enhance the selectivity and sensitivity for monoamine sensing[35–37]. We therefore incorporated metalloporphyrin, 5,10,15,20-tetrakis-(4′-aminophenyl) iron(III) porphyrin chloride or 5,10,15,20-tetrakis-(4′-aminophenyl) nickel(II) porphyrin into polyamic acid polymer as a precursor to produce nanoparticle-modified graphene networks through the laser carbonization process. Scanning electron microscope (SEM) images show that the laser carbonization process produced dense and interconnected graphene nanofibres with a resolution of 50–100 μm (Supplementary Fig. S2a–d). High-resolution transmission electron microscope (HRTEM) images of the laser-induced graphene show the characteristic 0.34-nm *d*-spacing (Extended Data Fig. 2e), whereas the Raman spectroscopy indicates that higher laser power produced more defects on the graphene (Extended Data Fig. 2f). The presence of nanoparticles (Fe_3O_4 and NiO) in the graphene network produced by the laser engraving process is confirmed by electron energy-loss spectroscopy (EELS) and HRTEM (Extended Data Fig. 3). The desired electrochemical properties, combined with the rapid laser patterning and the ease of transfer process enabled by SEBS, result in a versatile materials platform with high stretchability and rapid fabrication of arbitrary patterns (Supplementary Fig. S1).

As shown in Fig. 1b, the NeuroString developed for brain implantation is soft, elastic, thin and composed of long strings to minimize tissue damage, whereas that for the gut is on a single thin and elastic film to facilitate device operation and measurements over a much longer distance and a larger degree of movement (Supplementary Fig. S1). The patterned graphene–elastomer composite and the fabricated NeuroStrings can be easily stretched, twisted and even knotted (Supplementary Fig. S1). The NeuroString implanted in a mouse brain was rigidified using a pullulan coating to assist the implantation (Fig. 1c, the coating dissolves after implantation). The compatibility of NeuroStrings with soft organs is demonstrated by the highly flexible NeuroString non-invasively accessing the twisting colon of a mouse, as shown in a micro-computed tomography (μ-CT) image (Fig. 1d).

We first studied the deformation mechanism of the graphene–elastomer composite. μ-CT showed that the graphene nanofibres still maintained an interconnected 3D network after being transferred and embedded into the SEBS elastomer (Fig. 1e). When stretched to 100% strain, the graphene nanofibre network became aligned along the stretching direction, which may help to maintain the conductive pathways. We then characterized the stretchability of the free-standing composite induced by different laser power levels. Generally, a higher laser power led to an increase of graphene loading in the elastomer,

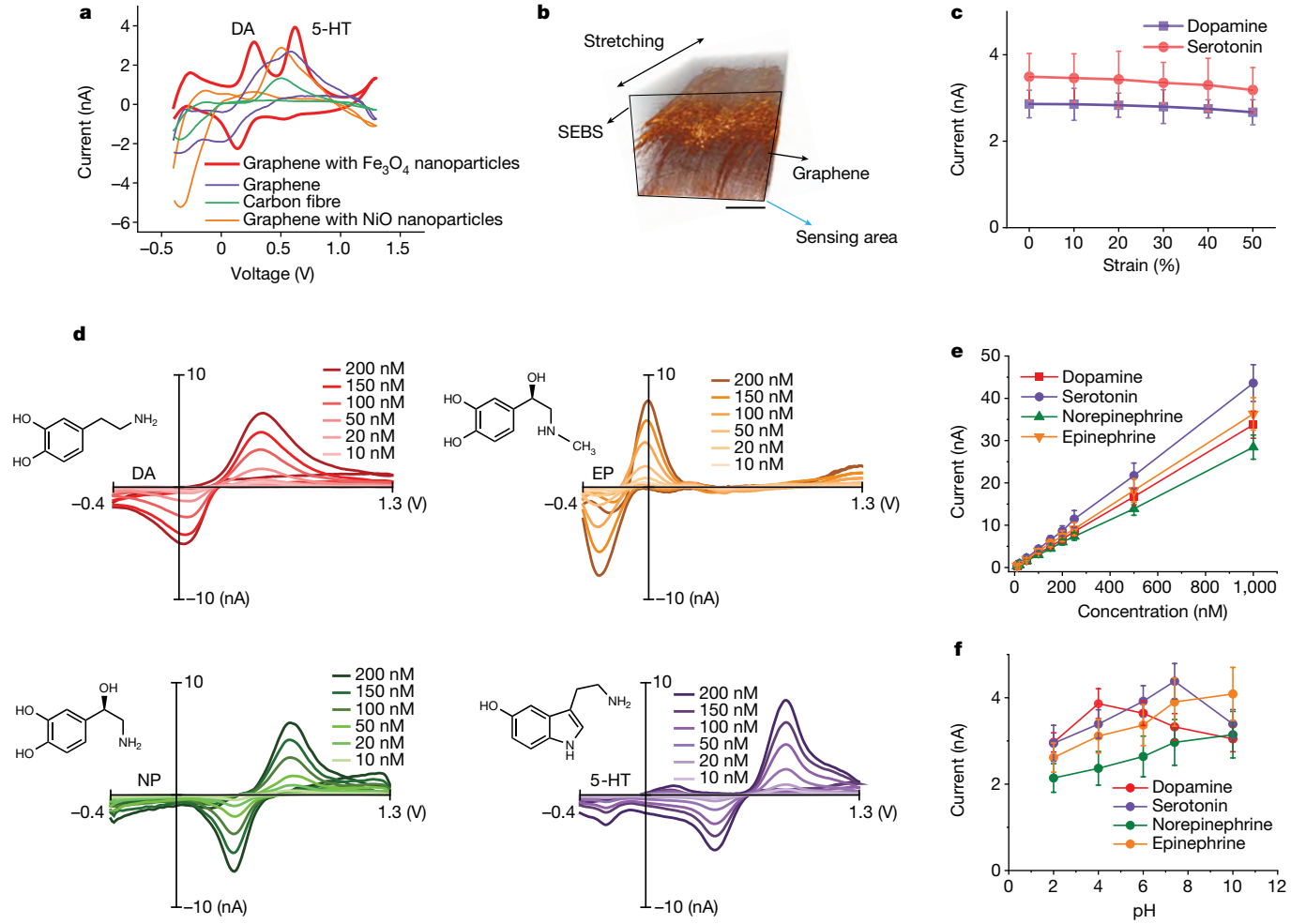

Fig. 2 | Electrochemical sensing performance of NeuroString electrode in solution. a, Comparison of the selectivity of different graphene electrodes (made of graphene with Fe_3O_4 nanoparticles, graphene with NiO nanoparticles and graphene only) and carbon fibre electrodes for simultaneously sensing DA and 5-HT using cyclic voltammetry (the individual voltammograms are shown in Extended Data Fig. 4d). **b**, X-ray tomography 3D reconstruction showing the cross section of the NeuroString electrode as the sensing area. The scale bar denotes 20 µm. **c**, Stable oxidation current peak of the electrodes, made of graphene with Fe_3O_4 nanoparticles, under different strains. The cyclic voltammetry is performed in a solution with 500 nM DA and 500 nM 5-HT in PBS buffer (pH 7.4) with a scan rate of 10 V s^{-1} (n = 6 electrodes). **d**, **e**, Concentration-dependent calibration response of NeuroString electrode to DA, EP, NP and 5-HT ranging from 10 to 200 nM in PBS buffer (pH 7.4) with a scan rate of 400 V s^{-1}. **f**, The current response to 100 nM analytes in PBS with different pH values (2, 4, 6, 7.4 and 10) with a scan rate of 400 V s^{-1}. Error bars are obtained from n = 6 different NeuroString electrodes examined in independent measurements.

as a thicker layer of polymer became carbonized (Supplementary Fig. S1). The tensile stress measurement in Fig. 1f shows that the graphene–elastomer composites exhibit a much higher strain to failure (>1,700%) compared with the neat SEBS elastomer. Graphene was reported to increase the Young's modulus when added in epoxy[34], but the graphene-in-elastomer composite showed a slightly decreased Young's modulus compared with that of the neat elastomer. In addition, the sheet resistance of the composite under 50% strain is stable, with a <200% change for products from all the laser powers (Fig. 1g, composite thickness: 50, 90 and 150 µm for laser powers of 6, 9 and 12 W, respectively). NeuroStrings produced with a laser power of 6 W to give a layer of graphene nanofibre with a thickness of about 50–80 µm were used in our following studies.

Next, we examined the electrochemical properties of the NeuroString electrodes. In vitro cyclic voltammetry measurements in the presence of both DA and 5-HT indicate that the graphene electrode decorated with Fe_3O_4 nanoparticles has the best selectivity and sensitivity to distinguish DA and 5-HT compared with the electrodes made by only graphene, graphene with NiO nanoparticles and commercial carbon fibres (Fig. 2a and Extended Data Fig. 4). As only the cross section of the graphene is used as sensing electrode (inset in Fig. 2b), we observed that stretching the device along different directions has minimal effect on the electrode impedance (<1,000 Hz), showed by a stable baseline under strain (Fig. S2). Similarly, the impedance of the NeuroString electrode was stable after being fabricated into arrays or under various pH (Supplementary Fig. S2). The NeuroString electrode also showed a stable oxidation current with a <10% decrease in amplitude when stretched to 50% strain (Fig. 2c), which affords stable and accurate monitoring of neurochemical dynamics in actively moving tissues and organs. NeuroString can sense several monoamine neurotransmitters, including DA, norepinephrine (NP), 5-HT and epinephrine (EP), with a FSCV detection limit of 5.6 nM, 7.2 nM, 3.5 nM and 6.6 nM, respectively (three times the standard deviation of the noise). A linear response curve ranging from 10 nM to 1 µM and a relatively stable current response across different pH are observed (Fig. 2c–e and Extended Data Fig. 4e, f). The linearity of FSCV sensing starts to decrease for concentrations above 1 µM, whereas chronoamperometry shows a better linearity for 5-HT sensing at the µM range (Extended Data Fig. 4g). NeuroString also allows simultaneous sensing of 5-HT and other catecholamines (norepinephrine and epinephrine), with a

selectivity in the sub-μM range (Extended Data Fig. 4h, i). Autoclave (121 °C) sterilization has a minimal effect on its sensory performance, which facilitated its in vivo use (Supplementary Fig. S2).

Next we used the NeuroString to monitor neurotransmitter dynamics in vivo in the mouse brain. The nucleus accumbens (NAc) is one of the main regions receiving projections from DA neurons in the ventral tegmental area (VTA). We stereotaxically injected Cre-dependent adeno-associated virus (AAV-DIO-ChR2) into the VTA of DAT-Cre mice to express light-sensitive channelorohopsin-2 (ChR2) specifically in DA neurons and implanted a three-channel NeuroString sensor ($90 \times 50\ \mu m^2$ in size) in the NAc and an optic fibre in the VTA for optogenetic stimulation (Fig. 3a). Using fast-FSCV (triangle waveform scanning from −0.4 V to 1.3 V), we achieved multiple-channel DA sensing in the NAc after delivering laser stimulus in the VTA (Fig. 3b, c). The peak of DA release ($[DA]_{max}$) under different stimulation frequencies was also examined (Fig. 3d, e). Fast detection of phasic DA release was achieved after repeated optostimulation (Fig. 3f), suggesting sub-second temporal resolution of the NeuroString. To test the capacity of NeuroString to sense behaviourally relevant endogenous DA release in freely moving animals, we implanted the NeuroString in the mouse NAc to measure the DA dynamics during reward learning and fear extinction. For the reward-learning experiments, freely moving mice were trained to associate an auditory cue with a water-ensuing reward (Fig. 3g–l). On the first training day (day 1), the NeuroString detected DA release triggered by the reward itself but not the reward-predicting cue (Fig. 3l). After 3 days of training, the mice can gradually associate the cue with the reward and a reward-predictive cue evoking DA release developed. We also subjected the mice to fear conditioning and extinction training using two different custom-made chambers inside a sound-attenuating box. Accompanied with the change of animal freezing levels across the association and extinction phases, we found that dopamine release increased after acute footshock during the conditioning phase and also at the end of the tone during the early extinction phase by NeuroString recording (Extended Data Fig. 5a–d), consistent with the role of dopamine signal in reinforcing and extinction learning[38].

Next we used optogenetic methods to activate the dorsal raphe nucleus (DRN) neurons and used the NeuroString to measure the optically stimulated 5-HT response in the basolateral amygdala (BLA) of the SERT-Cre mice (Fig. 3m). The peak amplitude of 5-HT release $[5\text{-HT}]_{max}$ can be enhanced with the frequency of photostimulation (Fig. 3n). Relative to baseline controls, systemic administration of fluoxetine, a selective serotonin reuptake inhibitor (SSRI), notably increased the clearance half-time of 5-HT (Fig. 3o–r).

We then used the NeuroString to examine the release of neurotransmitters induced by pharmacological compounds (Fig. 3s). We first performed ex vivo recording on acute brain slice to study the response of the catecholamine (CAT) and 5-HT under various drugs stimulation, including cocaine, amphetamine, 5-hydroxytryptophan (5-HTP) and fluoxetine. A concentric bipolar cluster microelectrode and a NeuroString electrode were positioned into the ventral striatum for electrical stimulation and neurochemical sensing, respectively. NeuroString detected the phasic CAT release evoked by electrical stimulation, with increased amplitude and duration by both cocaine and amphetamine, whereas the 5-HT signal was selectively enhanced by 5-HTP and fluoxetine application (Supplementary Fig. S3). We then examined the release of CAT and 5-HT at the ventral striatum evoked by intraperitoneal injection of cocaine and 5-HTP in living mice. Two oxidation peaks in the colour plot recorded by the NeuroString suggested the release of both CAT and 5-HT after co-administration of cocaine and 5-HTP (Fig. 3t). To further confirm the specificity, we injected fluoxetine after 5-HTP + cocaine co-injection and observed that the clearance time of 5-HT was selectively modified by the fluoxetine (Fig. 3u–x).

Chronic implantation and optogenetic probing showed that NeuroString can achieve reproducible DA signals evoked by optogenetic stimulation up to 16 weeks, demonstrating exceptional stability for long-term in vivo neurochemical sensing (Extended Data Fig. 5e–g). Immunohistology against the microglia marker Iba-1 (ionized calcium-binding adapter molecule) and the astrocyte marker GFAP (glial fibrillary acidic protein) showed that the soft NeuroString induced only slight elevation of GFAP and minimal overexpression of Iba-1 (Supplementary Fig. S4). The GFAP and Iba-1 signals were substantially lower than that caused by rigid silica fibre control (100 μm diameter), which is commonly used to encapsulate conventional carbon fibre electrodes. Together, these results indicated that the soft NeuroString showed better biocompatibility and evoked less adverse tissue response compared with conventional rigid probes.

In addition to neurochemical sensing in the CNS, NeuroString is uniquely suited for in vivo neurochemical sensing in the GI tract. 5-HT is an essential gut signalling molecule that contributes to the activation of intrinsic and extrinsic GI reflexes and has a strong effect on the microbiota[29] (Fig. 4a). In previous works, carbon fibres were able to measure the luminal or mucosal surface serotonin release and uptake of rodent intestine, which was usually dissected and pinned flat on a surface[39,40]. To study the 5-HT dynamics in active intestine, we first verified the mechanical compliance of the NeuroString in mouse intestine under ex vivo peristalsis motion. Whole mice colon tissue without content was placed into a Krebs-filled bath. Figure 4b shows that the NeuroString can readily interface with and attach to the mucosa of mouse colon as both the SEBS and the colon mucosa are soft and hydrophobic. Time-lapse images (Fig. 4c) showed that the mouse colon exhibited continuous contraction and relaxation when a NeuroString was placed in the lumen during electrochemical measurement (Supplementary Video S1). The colonic motility assay (Extended Data Fig. 6 and Supplementary Video S2) indicated that placing a NeuroString ($2\ cm \times 800\ \mu m \times 120\ \mu m$) in a mouse colon did not induce latency of the myoelectric slow-wave-induced mechanical contractions and colonic migrating motor complexes (CMMCs). By contrast, placing a flexible (but not stretchable) polyimide fibre with the same dimensions in the colon lumen delayed both the CMMCs and slow-wave-induced contractions, most probably resulting from the modulus mismatch and lack of stretchability (Fig. 4d–f). Behaviourally, the presence of the NeuroString in the colon did not affect the mobility of mice in the open-field assay or the faecal output (Extended Data Fig. 6). By contrast, the flexible polyimide control markedly reduced the mouse activity and faecal output. Haematoxylin and eosin (H&E) staining also showed that NeuroString electrodes induced minimal tissue damage, whereas placing polyimide fibre in the colon led to damage of the mucosa layer (Extended Data Fig. 6).

Enterochromaffin (EC) cells locate within the gut epithelia and store the largest pool of 5-HT in the body[41]. Thus a large amount of 5-HT is released from EC cells into the gut lumen in response to various stimuli and can be detected by the NeuroString through electrochemical measurements. The gut vagal afferents are particularly sensitive to mechanical stimuli, owing to the abundance of mechanoreceptors in the sensory endings of the GI tract wall to trigger 5-HT release and enhance peristaltic reflexes[29]. Real-time 5-HT recording using a NeuroString by chronoamperometry showed a stable 5-HT concentration during the peristalsis motion of the colon (Fig. 4g). However, recordings obtained with a commercial carbon fibre indicated obvious mechanically stimulated 5-HT releases during colon movements. This was consistent with a previous study of mechanically stimulated 5-HT release in the gut of the guinea pig[42]. We also observed that increasing the bath temperature from 37 °C to 42 °C can evoke elevation of 5-HT release in the colon lumen using an ex vivo assay (Fig. 4h, i). Taken together, these results confirmed that the mechanical compliance of the NeuroString is uniquely adequate to reduce disruptions to the physiological state of actively moving organs while maintaining high data recording fidelity.

5-HT can act as both a pro-inflammatory and an anti-inflammatory signalling molecule in the intestinal mucosa by means of activation of 5-HT receptors[43,44]. We next explored whether NeuroString can

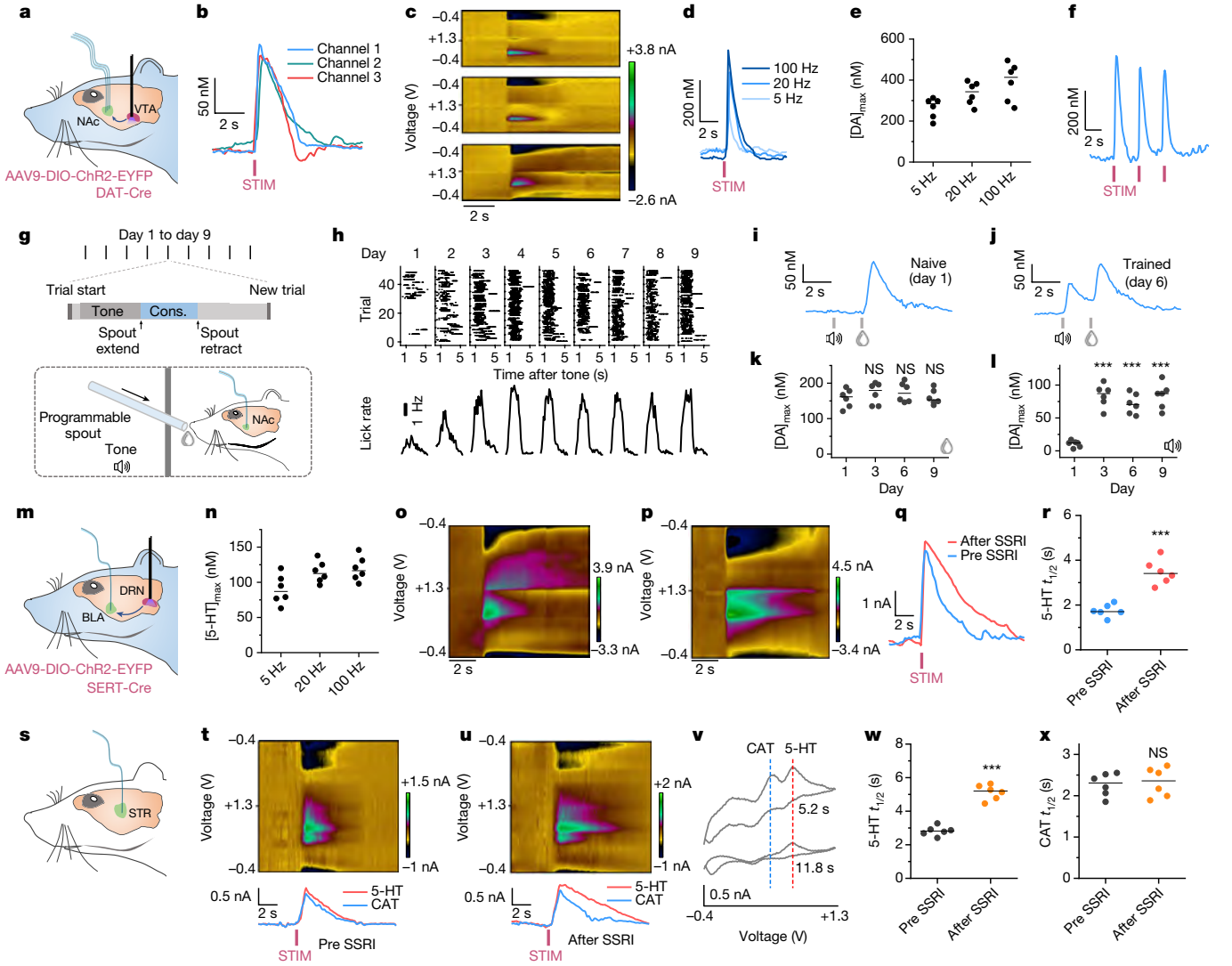

Fig. 3 | Neurochemical sensing in the brain. a, Schematic of dopamine sensing in the NAc by NeuroString sensor while optogenetically stimulating VTA dopaminergic neurons. Representative curves of estimated DA concentration versus time (**b**) and corresponding background-subtracted colour plots measured from a three-channel NeuroString through optogenetic stimulation (20 Hz with 15 pulses) (**c**). **d**, Representative traces of phasic DA release in the NAc under different stimulation frequencies (15 pulses). **e**, Calibrated DA peak concentration evoked by stimulation using different frequencies ($n = 6$ mice). **f**, Representative trace of phasic DA release under repetitive stimulation (20 Hz, 15 pulses). **g**, Experimental model for a Pavlovian reward learning task in freely moving mice. **h**, Representative lick raster plots from example mouse across nine conditioning sessions (upper) and corresponding average lick rate across nine conditioning sessions (lower). **i**, **j**, Exemplar time-aligned DA signals from a mouse in naive (**i**) and trained sessions (**j**). **k**, **l**, Group analysis of DA responses to unconditioned stimulus (water) (**k**) and conditioned stimulus (auditory cue) across trainings (**l**) ($n = 6$ mice). *P*-values: water: 0.3898 (day 3), 0.2425 (day 6) and 0.8826 (day 9); auditory cue: 0.0002 (day 3), 0.0001 (day 6) and 0.0004 (day 9). **m**, Schematic showing the serotonin measurements in the BLA with optogenetic stimulation using SERT-Cre mouse. **n**, Estimated $[5\text{-HT}]_{max}$ evoked by 15 pulse stimulation trainings applied at 5, 20 and 100 Hz ($n = 6$ mice). **o**, **p**, Representative colour plots showing 5-HT release evoked in the BLA by a 20-Hz, 15-pulse DRN stimulation before SSRI injection (**o**) and 30 min after SSRI injection (10 mg kg^{-1}) (**p**). **q**, Averaged concentration trace showing 5-HT release evoked by 20-Hz stimulation at baseline (blue line) and 30 min after SSRI (fluoxetine, red line) injection. **r**, Comparison of average clearance half-time $t_{1/2}$ at baseline and 30 min after SSRI injection ($n = 6$ mice). *P*-value: 0.0005. **s**, Schematic showing NeuroString in striatum for measuring CAT and 5-HT co-release. **t**, Representative colour plot (upper) and the corresponding estimated concentrations (lower) of CAT and 5-HT measured by NeuroString after administration of cocaine (15 mg kg^{-1}) + 5-HTP (15 mg kg^{-1}). **u**, Representative colour plot (upper) and the corresponding estimated concentrations (lower) of CAT and 5-HT measured by NeuroString after administration of cocaine (15 mg kg^{-1}) + 5-HTP (15 mg kg^{-1}) + SSRI (10 mg kg^{-1}). **v**, Representative cyclic voltammograms for detecting DA and 5-HT in the NAc 30 min after administration of cocaine (15 mg kg^{-1}) + 5-HTP (15 mg kg^{-1}) + SSRI (10 mg kg^{-1}). **w**, Comparison of average 5-HT clearance half-time $t_{1/2}$ at baseline and 30 min after SSRI injection ($n = 6$ mice). *P*-value: 0.000079. **x**, Comparison of average CAT clearance half-time $t_{1/2}$ at baseline and 30 min after SSRI injection ($n = 6$ mice). *P*-value: 0.7930. *P*-values are calculated by paired two-tailed Student's *t*-test: NS, $P > 0.05$; $^{*}P \le 0.05$; $^{**}P \le 0.01$; $^{***}P \le 0.001$.

non-invasively monitor the changes of 5-HT levels during the development of GI inflammation in a mouse model of inflammatory bowel disease. Feeding mice for 10 days with dextran sulfate sodium (DSS) in their drinking water induced acute colitis[45], as shown in the H&E staining of the mice colon (Extended Data Fig. 6). Colonic measurements using the NeuroString (acutely placed in the colon lumen during each test) showed elevated 5-HT levels in DSS but not saline-fed mice after 5 days of DSS treatment (Fig. 4k). The increase of 5-HT level for DSS mice was also confirmed by enzyme-linked immunosorbent assay (Extended Data Fig. 6). The increased availability of luminal 5-HT is consistent with

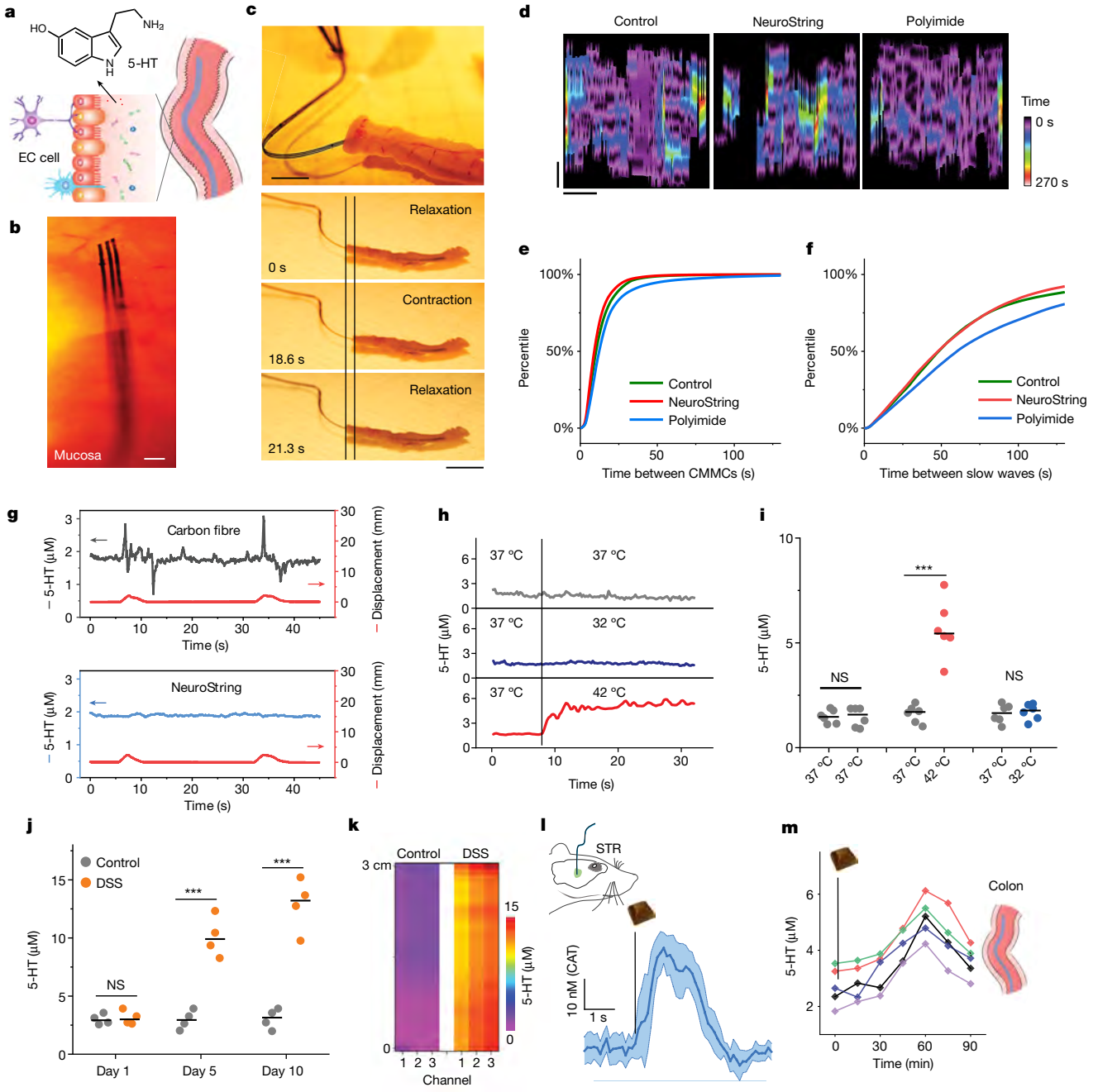

Fig. 4 | Neurochemical sensing in the GI system. a, Scheme showing 5-HT being released by the EC cell on the intestinal epithelium layer. **b**, Ex vivo image showing that the NeuroString can conform to the mucosa of mouse colon. The scale bar denotes 1 mm. **c**, Time-lapse images showing contraction and relaxation of the mouse colon during the neurochemical measurement. The scale bars denote 5 mm (top) and 1 cm (bottom). **d**, Representative spatiotemporal maps of the CMMC. Control data were obtained using a colonic motility assay without a device in the lumen. Spatiotemporal maps indicate the interval between CMMCs (*y*-axis) at each cross-sectional diameter (*x*-axis) along the colon length. The scale bars denote 100 s (vertical) and 10 mm (horizontal). CMMC intervals (**e**) and slow-wave induced contraction intervals mapped by video imaging colonic motility (**f**) (each curve shows the averaged measurement result obtained from colons of $n = 5$ biologically independent mice). **g**, Ex vivo chronoamperometry measurement of 5-HT concentration and the corresponding displacement (red) of mouse colon undergoing peristalsis motion (potential: +500 mV) using a NeuroString or commercial carbon fibres during the colon contracting motion. Representative traces (**h**) and histogram (**i**) of temperature change from 37 °C to 42 °C evoked 5-HT concentration change in mouse colon measured by NeuroString ($n = 6$ mice colons, *P*-values: 0.8190, 0.0004 and 0.1806). **j**, Mouse colon 5-HT concentration change measured by NeuroString during DSS-induced colitis development ($n = 4$ mice, *P*-values: 0.7348, 0.0073 and 0.0075). Each data point represents an average of five measurements inside this range at a distance of 0–3 cm from the anus of the mouse. **k**, Representative 5-HT concentration mapping of the mouse colon (3 cm from the anus) of a colitis mouse and a healthy mouse. Simultaneous DA and 5-HT measurement using chocolate as reward and nutrition stimulates for mice. Phasic CAT release in the striatum with intake of chocolate (error bar bands denote ±standard deviation of the measurement results obtained from $n = 5$ biologically independent mice) (**l**) and corresponding 5-HT level changes in the colon over time following intake of chocolate ($n = 5$ mice) (**m**). *P*-values are calculated by paired two-tailed Student's *t*-test: NS, $P > 0.05$; $^{*}P \leq 0.05$; $^{**}P \leq 0.01$; $^{***}P \leq 0.001$.

the increased number of EC cells associated with inflammation[46]. By mapping the colon luminal 5-HT using a multiple-channel NeuroString, we observed that healthy mice showed a gradual decrease in 5-HT level from the middle to the distal colon, whereas the 5-HT level in mice with colitis lacked such spatial distribution, with a much higher concentration level and higher variation, owing to the colon purulency (Fig. 4k). An average concentration difference of about 6% was also observed between different channels, indicating the local 5-HT heterogeneity. These results show that 5-HT can serve as a biomarker for gut inflammation, whereas the integration of the NeuroString can be used for inflammatory bowel disease diagnosis and studying the gut chemistry in humans. The flexibility of the NeuroString allows it to be wrapped on an endoscope to enable rapid mapping of the colon 5-HT by navigating the endoscope working channel while performing electrochemical sensing in a rat model (Extended Data Fig. 6f, g).

We also performed experiments using NeuroString to measure the kinetics of intestine luminal 5-HT in a pig model through acute experiments. Multichannel NeuroString can simultaneously measure different segments of the GI tract. We also examined drug-induced 5-HT release in the pig model and found that a cocktail drug of fluoxetine (SSRI) and methylene blue (MB, a monoamine oxidase inhibitor) led to 5-HT concentration increase in living miniature pigs (Extended Data Fig. 6). These results further validated the functionality of the device for real-time sub-second neurotransmitter measurements in different species and can be adopted to study the neurotransmitter kinetics in large animals. Last, we used the NeuroString sensors to simultaneously measure striatal CAT release and colon 5-HT changes in response to intake of chocolate in mouse, which is reward and nutrient. We detected reproducible release patterns of striatal CAT following intake of rewarding chocolate within seconds across animals, although an elevation of colonic 5-HT was also observed at 30–60 min after the nutrition uptake (Fig. 4k, l), a result consistent with the typical transit time of mouse gastrointestinal tract[47]. This result demonstrated the potential of using NeuroString for understanding neurotransmitter dynamics and their roles in the CNS–GI axis.

In summary, by developing a sensor based on the graphene–elastomer composite, we demonstrate that NeuroString functions as a soft bioelectronic interface to monitor the dynamics of monoamine neurotransmitters, including DA and 5-HT, in both the brain and the gut of living animals. With tissue-like mechanical properties, the NeuroString can interface acutely with the GI mucosa and is compatible with traditional medical inspection devices, such as endoscopy, for non-invasive biomolecular monitoring. NeuroString allows chronically stable and multiplexed neurochemical sensing in the mouse CNS. In the GI tract, the stretchability and softness of NeuroString offers high conformability with intestinal tissue without disturbing the peristaltic movement and without inducing undesired stimulation. The unique elastic features of NeuroString make it suitable for simultaneous monitoring of neurotransmitter signalling from both the central and the peripheral nervous systems, and potentially address current technical limitations in studying the dynamics of gut chemistry and its interplay with microbes. Although inheriting the limitations of the voltammetry method makes the sensitivity and selectivity of NeuroString in general worse than the latest genetically encoded fluorescence probes[1,11,12], such electrochemical methods are advantageous for translational use in humans[18,19]. NeuroString can also simultaneously sense multiple biomolecules at multiple locations. Further development will be dedicated to improving the spatial resolution of the sensor using microfabrication/nanofabrication, to improve its selectivity and multiplexity by incorporating different molecular recognition probes and eventually to integrate it with wireless electronics and to validate its long-term implantation performance. Combining the excellent mechanical properties with the versatility of chemical sensing provided by the graphene surface chemistry, we predict that the NeuroString platform will be readily adaptable for studying the dynamics of various signalling biomolecules and electrophysiological signals throughout the body in primates.

Online content

Any methods, additional references, Nature Research reporting summaries, source data, extended data, supplementary information, acknowledgements, peer review information; details of author contributions and competing interests; and statements of data and code availability are available at https://doi.org/10.1038/s41586-022-04615-2.

1. Patriarchi, T. et al. Ultrafast neuronal imaging of dopamine dynamics with designed genetically encoded sensors. *Science* **360**, eaat4422 (2018).
2. Nakatsuka, N. et al. Aptamer–field-effect transistors overcome Debye length limitations for small-molecule sensing. *Science* **362**, 319–324 (2018).
3. Kishida, K. T. et al. Subsecond dopamine fluctuations in human striatum encode superposed error signals about actual and counterfactual reward. *Proc. Natl Acad. Sci.* **113**, 200–205 (2016).
4. Wise, R. A. Dopamine, learning and motivation. *Nat. Rev. Neurosci.* **5**, 483–494 (2004).
5. Naughton, M., Mulrooney, J. B. & Leonard, B. E. A review of the role of serotonin receptors in psychiatric disorders. *Hum. Psychopharmacol.* **15**, 397–415 (2000).
6. Hyman, S. E. & Malenka, R. C. Addiction and the brain: the neurobiology of compulsion and its persistence. *Nat. Rev. Neurosci.* **2**, 695–703 (2001).
7. Russo, S. J. & Nestler, E. J. The brain reward circuitry in mood disorders. *Nat. Rev. Neurosci.* **14**, 609–625 (2013).
8. Cummings, J. L. Depression and Parkinson's disease: a review. *Am. J. Psychiatry* **149**, 443–454 (1992).
9. Spohn, S. N. & Mawe, G. M. Non-conventional features of peripheral serotonin signalling-the gut and beyond. *Nat. Rev. Gastroenterol. Hepatol.* **14**, 412–420 (2017).
10. Furness, J. B. The enteric nervous system and neurogastroenterology. *Nat. Rev. Gastroenterol. Hepatol.* **9**, 286–294 (2012).
11. Marvin, J. S. et al. An optimized fluorescent probe for visualizing glutamate neurotransmission. *Nat. Methods* **10**, 162–170 (2013).
12. Sun, F. et al. A genetically encoded fluorescent sensor enables rapid and specific detection of dopamine in flies, fish, and mice. *Cell* **174**, 481–496.e19 (2018).
13. Robinson, D. L., Venton, B. J., Heien, M. L. A. V. & Wightman, R. M. Detecting subsecond dopamine release with fast-scan cyclic voltammetry in vivo. *Clin. Chem.* **49**, 1763–1773 (2003).
14. Hashemi, P., Dankoski, E. C., Petrovic, J., Keithley, R. B. & Wightman, R. M. Voltammetric detection of 5-hydroxytryptamine release in the rat brain. *Anal. Chem.* **81**, 9462–9471 (2009).
15. Schwerdt, H. N. et al. Long-term dopamine neurochemical monitoring in primates. *Proc. Natl Acad. Sci.* **114**, 13260–13265 (2017).
16. Taylor, I. M. et al. Enhanced dopamine detection sensitivity by PEDOT/graphene oxide coating on in vivo carbon fiber electrodes. *Biosens. Bioelectron.* **89**, 400–410 (2017).
17. Clark, J. J. et al. Chronic microsensors for longitudinal, subsecond dopamine detection in behaving animals. *Nat. Methods* **7**, 126–129 (2010).
18. Moran, R. J. et al. The protective action encoding of serotonin transients in the human brain. *Neuropsychopharmacology* **43**, 1425–1435 (2018).
19. Bang, D. et al. Sub-second dopamine and serotonin signaling in human striatum during perceptual decision-making. *Neuron* **108**, 999–1010.e6 (2020).
20. Minev, I. R. et al. Electronic dura mater for long-term multimodal neural interfaces. *Science* **347**, 159–163 (2015).
21. Vázquez-Guardado, A., Yang, Y., Bandodkar, A. J. & Rogers, J. A. Recent advances in neurotechnologies with broad potential for neuroscience research. *Nat. Neurosci.* **23**, 1522–1536 (2020).
22. Hong, G. & Lieber, C. M. Novel electrode technologies for neural recordings. *Nat. Rev. Neurosci.* **20**, 330–345 (2019).
23. Deng, J. et al. Electrical bioadhesive interface for bioelectronics. *Nat. Mater.* **20**, 229–236 (2021).
24. Frank, J. A., Antonini, M. J. & Anikeeva, P. Next-generation interfaces for studying neural function. *Nat. Biotechnol.* **37**, 1013–1023 (2019).
25. Lee, S. et al. Ultrasoft electronics to monitor dynamically pulsing cardiomyocytes. *Nat. Nanotechnol.* **14**, 156–160 (2019).
26. Terem, I. et al. Revealing sub-voxel motions of brain tissue using phase-based amplified MRI (aMRI). *Magn. Reson. Med.* **80**, 2549–2559 (2018).
27. Spencer, K. C. et al. Characterization of mechanically matched hydrogel coatings to improve the biocompatibility of neural implants. *Sci. Rep.* **7**, 1952 (2017).
28. Schwerdt, H. N. et al. Subcellular probes for neurochemical recording from multiple brain sites. *Lab Chip* **17**, 1104–1115 (2017).
29. Mazzuoli-Weber, G. & Schemann, M. Mechanosensitivity in the enteric nervous system. *Front. Cell. Neurosci.* **9**, 408 (2015).
30. Patel, B. A., Bian, X., Quaiserová-Mocko, V., Galligan, J. J. & Swain, G. M. In vitro continuous amperometric monitoring of 5-hydroxytryptamine release from enterochromaffin cells of the guinea pig ileum. *Analyst* **132**, 41–47 (2007).
31. Osorio, N. & Delmas, P. Patch clamp recording from enteric neurons in situ. *Nat. Protoc.* **6**, 15–27 (2011).
32. Bucher, E. S. & Wightman, R. M. Electrochemical analysis of neurotransmitters. *Annu. Rev. Anal. Chem.* **8**, 239–261 (2015).
33. Xu, C., Wu, F., Yu, P. & Mao, L. *In vivo* electrochemical sensors for neurochemicals: recent update. *ACS Sens.* **4**, 3102–3118 (2019).

34. Kinloch, I. A., Suhr, J., Lou, J., Young, R. J. & Ajayan, P. M. Composites with carbon nanotubes and graphene: an outlook. *Science* **362**, 547–553 (2018).
35. Sun, D. et al. Electrodeposition synthesis of a NiO/CNT/PEDOT composite for simultaneous detection of dopamine, serotonin, and tryptophan. *Sens. Actuators B Chem.* **259**, 433–442 (2018).
36. Yang, W. et al. Enhancing electrochemical detection of dopamine *via* dumbbell-like FePt–Fe_3O_4 nanoparticles. *Nanoscale* **9**, 1022–1027 (2017).
37. Fernandes, D. M. et al. Novel electrochemical sensor based on N-doped carbon nanotubes and Fe_3O_4 nanoparticles: simultaneous voltammetric determination of ascorbic acid, dopamine and uric acid. *J. Colloid Interface Sci.* **432**, 207–213 (2014).
38. Salinas-Hernández, X. I. et al. Dopamine neurons drive fear extinction learning by signaling the omission of expected aversive outcomes. *eLife* **7**, e38818 (2018).
39. Bertrand, P. P., Hu, X., Mach, J. & Bertrand, R. L. Serotonin (5-HT) release and uptake measured by real-time electrochemical techniques in the rat ileum. *Am. J. Physiol. Gastrointest. Liver Physiol.* **295**, G1228–G1236 (2008).
40. Bertrand, P. P. Real-time measurement of serotonin release and motility in guinea pig ileum. *J. Physiol.* **577**, 689–704 (2006).
41. Bertrand, P. P. & Bertrand, R. L. Serotonin release and uptake in the gastrointestinal tract. *Auton. Neurosci.* **153**, 47–57 (2010).
42. Bertrand, P. P. Real-time detection of serotonin release from enterochromaffin cells of the guinea-pig ileum. *Neurogastroenterol. Motil.* **16**, 511–514 (2004).
43. Mawe, G. M. & Hoffman, J. M. Serotonin signalling in the gut—functions, dysfunctions and therapeutic targets. *Nat. Rev. Gastroenterol. Hepatol.* **10**, 473–486 (2013).
44. Gershon, M. D. & Tack, J. The serotonin signaling system: from basic understanding to drug development for functional GI disorders. *Gastroenterology* **132**, 397–414 (2007).
45. Okayasu, I. et al. A novel method in the induction of reliable experimental acute and chronic ulcerative colitis in mice. *Gastroenterology* **98**, 694–702 (1990).
46. Linden, D. R., Chen, J. X., Gershon, M. D., Sharkey, K. A. & Mawe, G. M. Serotonin availability is increased in mucosa of guinea pigs with TNBS-induced colitis. *Am. J. Physiol. Gastrointest. Liver Physiol.* **285**, 761–768 (2003).
47. Padmanabhan, P., Grosse, J., Asad, A. B. M. A., Radda, G. K. & Golay, X. Gastrointestinal transit measurements in mice with ^{99m}Tc-DTPA-labeled activated charcoal using NanoSPECT-CT. *EJNMMI Res.* **3**, 60 (2013).

Methods

Materials preparation

Synthesis of polymer precursor containing Fe or Ni metalloporphyrin. 5,10,15,20-tetrakis-(4′-aminophenyl) iron(III) porphyrin chloride and 5,10,15,20-tetrakis-(4′-aminophenyl) nickel(II) porphyrin were synthesized according to a previously reported protocol[48]. 100 mg of pyromellitic dianhydride (4.59×10^{-1} mM) was dissolved in 1.4 ml N-methyl-2-pyrrolidone at 100 °C. The solution was cooled to room temperature. Then, 180 mg of 5,10,15,20-tetrakis-(4′-aminophenyl) iron(III) porphyrin chloride (2.30×10^{-1} mM), three drops of isoquinoline and 1.4 g of polyamic acid solution (poly(pyromellitic dianhydride-co-4,4′-oxydianiline)) were introduced in sequence under stirring at room temperature. Pyromellitic dianhydride, isoquinoline and polyamic acid solution, 15.0–16.0 wt.% in N-methyl-2-pyrrolidone) were purchased from Sigma-Aldrich without any further purification before use.

Device fabrication

NeuroString for brain neurochemical sensing. The NeuroString fabrication process is on the basis of direct laser carbonization of the above polyimide polymer precursor (containing metalloporphyrin) into conductive nanoporous graphene networks decorated with nanoparticles (Extended Data Fig. 1a). The design layout of the multichannel NeuroString for brain neurochemical sensing is shown in Extended Data Fig. 1b. Electrical-grade Kapton polyimide film (McMaster-Carr, 12″ wide, 0.0050″ thick, 12″ long) was used as the initial substrate. The polyimide film was first cut into a rectangle shape with dimensions 3″ × 2″. The surface of the polyimide film was then cleaned with oxygen plasma (Technics Micro-RIE Series 800, 150 W, 200 mtorr) for 2 min. Then the prepared metalloporphyrin-containing polyamic acid solution was uniformly coated (50 μl cm^{-2}) on the polyimide substrate using a razor blade (step 1 in Extended Data Fig. 1c). Owing to the high viscosity of the precursor solution, this preparation was left in air for 1 h to form a uniform liquid film with a flat surface. Then the sample was loaded on a hotplate (100 °C) for 1 h to remove all the solvent. The film was then annealed at 150 °C for 5 min and at 250 °C for 1 h (step 2 in Extended Data Fig. 1c). Then the resulting film surface was laser engraved by an Epilog Fusion M2 CO_2 laser (step 3 in Extended Data Fig. 1c) following a reported method on laser-induced graphene[49]. A laser power of 6 W was used with a raster speed of 25%. After laser engraving, the film turned into a nanoporous graphene network decorated with nanoparticles. A High Power Density Focusing Optics (HPDFO) lens with a focal point of 0.001″ (25.4 μm) can be used improve the resolution of the engraving.

To prepare the NeuroString, a solution containing SEBS in toluene (Asahi Kasei Tuftec H1062, 0.1 g ml^{-1}) was drop-casted on the graphene networks (100 μl cm^{-2}) and then placed in a desiccator and pumped with a house vacuum for 5 min to remove all the gas bubbles. After allowing the toluene solvent to evaporate overnight, the graphene–SEBS composite was peeled off from the polyimide, flipped to expose graphene on top and placed on another glass substrate (step 4 in Extended Data Fig. 1c). Tape was used to cover the interconnect area and another SEBS layer (H1062, 0.1 g ml^{-1} in toluene) was spin-coated on top at 1,000 rpm, to form a stretchable encapsulation layer (step 5 in Extended Data Fig. 1c). After removal of the tape, the film was attached to a glass slide and laser cutting was used to define the individual separated electrodes with a width of 50–90 μm (step 6 in Extended Data Fig. 1c). A laser power of 30 W was used to cut the undesired part and to form small individual electrodes. Then the electrode was dip-coated with another block copolymer solution (Kuraray LA3320, 0.1 g ml^{-1} in acetone) to fully encapsulate the sidewalls of graphene electrodes (step 7 in Extended Data Fig. 1c). Then acetone was used to dissolve the LA3320, so as to not induce any dissolution of the formed electrodes and substrate.

For implantation in the brain, the NeuroString was dip-coated in a pullulan solution (0.3 g ml^{-1}) and dried overnight on a Teflon film to form the shuttle layer (step 8 in Extended Data Fig. 1c). Finally, the tips of electrodes were cut using a razor blade to expose the cross sections of the graphene (step 9 in Extended Data Fig. 1c). To fully expose the graphene, the cross-sectional surfaces of electrodes were oxygen plasma-treated (Technics Micro-RIE Series 800, 150 W, 200 mtorr) for 2 min. To avoid any interference of the ascorbic acid and biofouling from the biological fluids, the tips of the electrodes were finally dipped in a Nafion solution (0.5% in water/ethanol) to form a Nafion coating before use. Once the device was implanted in the brain tissue, the NeuroString was released after the pullulan dissolved away to give a soft implanted electrode (step 10 in Extended Data Fig. 1c). The electronic design was created with CorelDRAW software.

NeuroString for gut neurochemical sensing. The NeuroString fabrication process is on the basis of direct laser carbonization of the above polyimide polymer precursor (containing metalloporphyrin) into conductive nanoporous graphene networks decorated with nanoparticles (Extended Data Fig. 1a). The design layout of the multichannel NeuroString for gut neurochemical sensing is shown in Extended Data Fig. 1d. Electrical-grade Kapton polyimide film (McMaster-Carr, 12″ wide, 0.0050″ thick, 12″ long) was used as the initial substrate. The polyimide film was first cut into a rectangle shape with dimensions of 3″ × 2″. The surface of the polyimide film was then cleaned with oxygen plasma (Technics Micro-RIE Series 800, 150 W, 200 mtorr) for 2 min. Then the prepared metalloporphyrin-containing polyamic acid solution was uniformly coated (50 μl cm^{-2}) on the polyimide using a razor blade (step 1 in Extended Data Fig. 1d). Leaving the solution in air for 1 h gave a uniform solution coating. Then the sample was placed on a hotplate (100 °C) for 1 h to remove all the solvent. The film was then annealed at 150 °C for 5 min and at 250 °C for 1 h (step 2 in Extended Data Fig. 1). Then individual electrodes (width about 120–220 μm) were directly patterned on the polyimide surface using the laser engraving by an Epilog Fusion M2 CO_2 laser (step 3 in Extended Data Fig. 1) following a reported method on laser-induced graphene[49]. A laser power of 6 W was used with a raster speed of 25%. After laser engraving, the film coating was turned into a nanoporous graphene network decorated with nanoparticles.

Next, a SEBS solution (H1062, 0.1 g ml^{-1} in toluene) was uniformly drop-casted on the graphene network (100 μl cm^{-2}) and then placed in a desiccator and pumped with a house vacuum for 5 min to remove all the possible gas bubbles from the SEBS solution. After allowing the toluene solvent to evaporate overnight, the formed graphene–SEBS composite was peeled off from the polyimide substrate, flipped to expose graphene on top and placed on another glass substrate (step 4 in Extended Data Fig. 1). Tape was used to cover the interconnect area and another SEBS layer (H1062, 0.1 g ml^{-1} in toluene) was spin-coated on top at 1,000 rpm, to form a stretchable encapsulation layer (step 5 in Extended Data Fig. 1). After removal of the tape, the interconnect-encapsulated film was attached to a glass slide and laser cutting was used to define the probes (step 6 in Extended Data Fig. 1). A CO_2 laser with a power of 30 W was used to cut away the undesired part.

For easier placing in the mouse gut, the NeuroString was dip-coated in a pullulan solution (0.1 g ml^{-1}) and dried overnight on a Teflon film to form the shuttle layer (step 7 in Extended Data Fig. 1). Finally, the tips of electrodes were cut using a razor blade to expose the cross sections of the graphene (step 8 in Extended Data Fig. 1). To fully expose the graphene, the cross-sectional surfaces of electrodes were oxygen plasma-treated (Technics Micro-RIE Series 800, 150 W, 200 mtorr), for 2 min, making sure that the sensing electrode opening is facing up towards the plasma treatment in this process. To avoid any interference of the ascorbic acid and biofouling from the biological fluids, the tips of the electrodes were finally dipped in a Nafion solution (0.5% in water/ethanol) to form a Nafion coating before use. Once the device was in the gut tissue, dissolving of the pullulan released the NeuroString as a soft implant (step 9 in Extended Data Fig. 1). The electronic design was created with CorelDRAW software.

Characterization

Morphological and compositional characterization. The SEM images were taken by a FEI XL30 Sirion SEM (5 kV). The LabRAM HR Evolution microscope (HORIBA Scientific) was used for Raman spectroscopy with 532-nm or 633-nm excitation and a 1,800 grooves per mm grating. HRTEM images were taken on a FEI Titan 80-300 environmental (scanning) electron microscope (E(S)TEM). Laser-induced graphene was scraped off and sonicated in ethanol before being transferred onto a copper TEM grid. The EDS/EELS elemental mappings were acquired using a Gatan Quefina dual-EELS spectrometer with an energy dispersion of 0.1 eV per channel. To minimize possible electron beam irradiation effects, all the EELS and EDS spectra demonstrated in this project were acquired from areas without pre-beam irradiation. X-ray photoelectron spectroscopy was performed on a PHI VersaProbe Scanning XPS Microprobe.

Micro X-ray computed tomography. Non-destructive CT reconstructions of the graphene–elastomer composite and the NeuroString in mouse colon were performed with a ZEISS Xradia 520 Versa X-ray microscope (Carl Zeiss AG). 1% iodine metal (I_2 dissolved in 100% ethanol) solution was used as the staining solution to increase the contrast of the device[50]. To stain the graphene networks, the iodine metal solution was directly dropped on the laser-induced graphene networks. After 10 min ethanol solvent evaporation, SEBS solution (H1062, 0.1 g ml^{-1} in toluene) was drop-cast on the graphene networks and then placed in a desiccator for 5 min to remove all the possible gas bubbles from the SEBS solution. After evaporation of the toluene solvent overnight, the formed graphene–SEBS composite was peeled off from the polyimide substrate, flipped to expose graphene on top and placed on another glass substrate. A CO_2 laser with power 30 W was used to cut the composite into small fibres with a diameter of about 200 μm for CT scanning. A home-made acrylic stage was used to allow the fibre to be stretched and imaged in the CT scanner. Similarly, to image the NeuroString in the mouse colon, iodine metal solution (I_2 dissolved in 100% ethanol) was directly dropped on the laser-induced graphene networks before the SEBS encapsulation process. An exposure time of 10 s was used with an acceleration voltage of 30 kV. A total of 2,501 CT scans was taken at 30 kV to create a 3D rendering of the interior morphology of the samples. The projection images were reconstructed into 3D images and processed using the software Dragonfly (Object Research Systems).

Mechanical property characterization. The mechanical properties of free-standing graphene–SEBS composite films with a thickness of about 50 μm were studied using an Instron 5565 tester with a 100-N loading cell. The samples were glued between compression plates. The width and length of the film were measured by a caliper. The thickness was measured by an optical microscope. A strain rate of 5% min^{-1} was used for mechanical testing if not otherwise indicated. The composite films had rectangular symmetry with a sample size of 10 × 2 mm.

Electrical and electrochemical characterization. To measure the conductivity of the graphene–SEBS composites during stretching, samples were attached to a home-made stretching station attached to an LCR meter (Keysight Technologies E4980). Silver epoxy was used to make contacts. A graphene–SEBS composite with dimensions 5 × 10 mm^2 was used to measure the square resistivity, while the stretching state was stretched by 2 mm in each step. The neurotransmitter sensing is on the basis of FSCV[14,17,32]. Electrochemical measurements were performed with a portable potentiostat PalmSens4 built with impedance spectroscopy, FSCV and a four-channel multiplexer. The electrochemical impedance of the NeuroString and FSCV were measured in the phosphate-buffered saline (PBS) buffer solution (pH 7.4). The potentiostatic electrochemical impedance spectroscopy was measured with a sine wave (frequency from 1 Hz to 1 MHz) and a signal amplitude of 10 mV. The FSCV was performed at different scan rates from 10 V s^{-1} to 400 V s^{-1} with a triangular waveform (−0.4 to 1.3 V, interval from 1 to 100 ms, depending on the scanning parameters) relative to the Ag/AgCl reference electrode placed in 3 M KCl. Selective neurotransmitter sensing can be achieved with a scan rate from 10 to 50 V s^{-1}, whereas increasing the scan rate to 500 V s^{-1} will give better sensitivity. Depending on the size of the electrode, the background current varies from 100 to 2,000 nA. For comparison, carbon fibre electrodes with a tip diameter of 10 μm were ordered from World Precision Instruments (Carbon Fiber Electrode, L 500 μm). Owing to the background current variation of each electrode, the background-subtracted Faradic currents response was normalized to a background current of 1,000 nA for comparison. Because the monoamine analytes in aqueous solution can be easily oxidized, the analyte solution used in the tests should be made directly before that testing and it is preferred to pump nitrogen to the PBS buffer for 2 h to remove the oxygen before making the solution. To stabilize the recording electrode, a triangular waveform was applied to the electrode at a frequency of 60 Hz for least 1 h to reduce the drifting[32,51,52]. A functioning electrode should have a stable capacitive background response during cyclic voltammetry scanning, as shown in Extended Data Fig. 4b.

Animal studies

Surgery for implantation of NeuroString into the mice brain and viral expression. All surgical procedures for mice were performed in accordance with protocols approved by the Institutional Animal Care and Use Committee (IACUC) at Stanford University. All the channels of the NeuroString were calibrated by measuring the normalized oxidation current at different analyte concentrations (10–200 nM in PBS) and then continuously scanned using FSCV (10–400 V s^{-1}, triangle wave, −0.4 to 1.3 V) for 1 h to ensure that there is no obvious drifting of the background current (<1% over 250 scans) before implantation. Mice were anaesthetized with a ketamine cocktail (100 mg kg^{-1} ketamine and 10 mg kg^{-1} xylazine, intraperitoneally) and placed in a stereotactic frame (Stoelting #51600). A heating pad was used to maintain the body temperature of the mice. A midsagittal incision was placed slightly anterior and posterior of bregma and lambda, respectively. Craniotomies (Stoelting #51449) were stereotaxically guided to place the NeuroString (with pullulan coating as the shuttle material) into the NAc (+1.18 AP, +0.6 ML, −4.2 DV) or the BLA (−1.34 AP, +2.9 ML, −4.7 DV) and then fixed with dental cement. A chloritized silver reference electrode (Ag/AgCl) was implanted ipsilaterally into the cortex area for each animal[17]. Following surgery, mice received analgesia that consisted of either ibuprofen (100 mg kg^{-1}) or buprenorphine (1 mg kg^{-1}). For all surgical procedures, animals were allowed to fully recover for at least two weeks before chronic recordings.

For the optogenetic stimulation experiments, 200 nl of concentrated adeno-associated virus encoding Cre-inducible channelrhodopsin-2 (AAV9-DIO-ChR2-EYFP; University of Pennsylvania Vector Core) was unilaterally injected into the VTA (−3.28 AP, +0.4 ML, −4.3 DV) of DAT-Cre animals (The Jackson Laboratory, No. 006660) or the DRN of SERT-Cre animals (The Jackson Laboratory, No. 014554) at an angle of 10° (−4.6 AP, 0 ML, −3.1 DV). Then, immediately following viral injection, a fabricated fibre optic was implanted above the injection site (VTA: −3.28 AP, +0.4 ML, −4.1 DV; DRN: −4.6 AP, 0 ML, −2.9 DV) and affixed to the skull using dental cement.

Neurotransmitter sensing in the mice brain. The monoamine level was recorded using FSCV. To stabilize the recording electrode, a triangular waveform was applied to the electrode at a frequency of 60 Hz for at least 1 h before each recording session[32,51,52]. The cycling frequency was then reduced to 10 Hz for 30 min or until a stable background was detected before initiation of the recording session. During this 'cycling' period, mice remained in their home cage. Voltammetric electrodes were

validated for functionality and for data inclusion using two criteria[52]: electrodes with a background current above 100 nA and background signal-to-noise ratio above 250:1; the background current is stable with a drift <1% over 250 scans. The first ten scans before stimulation were averaged as the background. The variable background drift was subtracted for each recording to eliminate the noise fluctuation during subsequent analysis. Voltammetric analysis was conducted using PSTrace 5.6 software, MATLAB and Origin.

Optogenetic stimulation. For optogenetic stimulation, dopaminergic neurons or serotoninergic neurons were stimulated using a laser (Laserglow, 473 nm, 5 mW, 1 s at 5, 20, 50 or 100 Hz). The dopamine or serotonin level was recorded during the stimulation using FSCV, which consisted of a triangular waveform (−0.4 to 1.3 V and back at 400 V s^{-1}) applied to the tip of the sensing electrode with a frequency of 10 Hz.

Drug effect. Drug-induced neurotransmitter release was performed using DAT-Cre animals. Neurochemical measurement was recorded after the drug injection using FSCV, which consisted of a triangular waveform (−0.4 to 1.3 V) with a relatively reduced scanning speed of 20 V s^{-1} and a frequency of 5 Hz. The method for evoking simultaneous release of serotonin and dopamine was achieved by a published method using a synthetic precursor of serotonin, 5-HTP, to increase the amount of serotonin in the dopamine terminals of the brain[53–55]. First, (S)-3-(3,4-dihydroxyphenyl)-2-hydrazino-2-methylpropionic acid monohydrate (carbidopa), which prevents the 5-HTP from being converted into serotonin before it reaches the brain, was intraperitoneally injected (25 mg kg^{-1}) if 5-HTP would be administered later. Thirty minutes later, cocaine (15 mg kg^{-1}), 5-HTP (500 mg kg^{-1}), a cocktail drug containing cocaine and 5-HTP or a cocktail drug containing cocaine, 5-HTP and fluoxetine (10 mg kg^{-1}) was intraperitoneally injected. As a control, saline was injected on separate days. Neurochemical measurement was performed at 10 min after the drug injection by FSCV.

Pavlovian cued-reward learning task. Six DAT-Cre animals with NeuroString implantation into the NAc were trained to lick a water spout after an auditory tone to obtain water in a custom-made chamber (30 × 35 mm). The chamber was equipped with a retractable spout in the centre of one wall and an auditory loudspeaker on the other side of the same wall. Mice were deprived from water and habituated to the chamber for 2 days. During the habituation, the animals reliably licked the spout to obtain the water. After the habituation, the cued-reward training began. In each trial, an auditory tone (4 kHz) was delivered for 2 s, followed by the extension of the water spout and a 4-s lick detection period. During this period, mice needed to lick the spout to trigger the delivery of 6 µl of water. Mice had a consumption period of 2 s after water delivery, followed by retraction of the spout and a random inter-trial interval (ITI) (17–27 s). If mice failed to lick during the lick-detection period, the spout was retracted immediately after this period and ITI was counted. The behaviour training and lick events were controlled and recorded by custom-written MATLAB code. FSCV recording was performed at 400 V s^{-1}. Mice were trained for 50 trials every day and water was supplied to ensure they received 1 ml of water every day (including the amount obtained during training) before going back to their home cage.

Fear extinction learning task. Five DAT-Cre animals with NeuroString implantation into the NAc were used in this study. Fear conditioning and extinction were performed in two different custom-made contexts inside a sound-attenuating box (Med Associates). All mice were habituated to the context A (a square chamber with an electrical grid floor) on day 1. An auditory tone (4 kHz, 10 s) was played five times with a random ITI (60–100 s). On day 2, mice were subjected to fear conditioning, consisting of five pairs of conditioned stimuli (CS, 4-kHz tone, 10 s) with an unconditioned stimulus (footshock, 0.35 mA, 1 s) in context A. The unconditioned stimuli occurred immediately after the termination of CS. The random ITI ranged from 60 to 100 s between each pair. Twenty-four hours later, mice received an extinction training in context B (a triangular chamber). Only the auditory tone (4 kHz, 10 s) was played in each trial. Mice were videotaped for analysing the freezing level in response to the CS. FSCV recording was performed at 400 V s^{-1} during each day.

Neurochemical sensing in the mice brain slices. One-month-old wild-type mice were used for slice experiments. Coronal 250-µm slices containing the NAc were prepared using a vibratome (Leica VT1000S) in an ice-cold cutting solution (in mM): sucrose 213, KCl 2.5, NaH_2PO_4 1.25, $MgSO_4$ 10, $CaCl_2$ 0.5, $NaHCO_3$ 26 and glucose 11 (300–305 mOsm). Slices were incubated in the artificial CSF containing the following (in mm): NaCl 126, KCl 2.5, NaH_2PO_4 1.25, $MgCl_2$ 2, $CaCl_2$ 2, $NaHCO_3$ 26 and glucose 10 (300–305 mOsm) at 34 °C to recover for 30 min and then kept in the artificial CSF at room temperature for at least 30 min before recording. To induce and detect the release of dopamine, a concentric bipolar cluster microelectrode (FHC, Inc.) and a NeuroString electrode were positioned in the ventral striatum. FSCV recording was performed at 10 V s^{-1} before drug perfusion or at 10 min after drug perfusion. The electrical stimuli (200 µA, 20 Hz, 0.5 s) was delivered five times with a 10-s interval between each stimulus for each FSCV recording. Four drugs were used to test their dosage effect on the evoked release of dopamine: amphetamine (1, 5, 10 µM), cocaine (1, 5, 10 µM), 5-HTP (1, 5, 10 µM) and fluoxetine (5, 10, 50 µM).

Serotonin sensing in mouse colon. Mice were euthanized by cervical dislocation. The abdomen was immediately opened and the entire colon from the caecum to the terminal rectum was removed. In all experiments, the full-length colon was placed in a Petri dish filled with carbogen-gassed (95% O_2/5% CO_2) Krebs solution (25–30 °C; in mM concentrations: NaCl 118, KCl 4.7, NaH_2PO_4 1, $NaHCO_3$ 25, $MgCl_2$ 1.2, D-glucose 11, $CaCl_2$ 2.5). Residual pellets were gently flushed from the colon using Krebs solution. A NeuroString was placed in the colon using pullulan as the shuttle material. Chronoamperometry with a potential of 600 mV was used to monitor the serotonin overflow. A Ag/AgCl wire was placed in the flow bath as the reference electrode. The heating and cooling of the buffer environment was achieved by a flow cell with a thermostat to control the temperature. The graphene electrodes of the NeuroString were calibrated by measuring the temperature-dependent oxidation current of serotonin solution in a water bath.

Serotonin sensing in living pigs. Female juvenile Yucatan miniature pigs (*Sus scrofa*, $n = 6$) aged 6–9 weeks and weighing 10 kg from breeder S&S Farms (Ramona, CA) were used in this study. NeuroString sensors were applied to the GI tract to record enteric serotonin levels. Briefly, all pigs were fasted overnight, placed under general anaesthesia using vaporized isoflurane and connected to vital-sign monitors during this terminal procedure. A midline laparotomy incision was made to expose the viscera. Krebs/PBS buffer was infused into the porcine intestine to flush the contents before sensing. The ligament of Treitz was identified to locate the duodenum and jejunum and the ileocecal valve was found to designate the ileum. Caecum and spiral colon were also exposed. Soft NeuroString sensors were applied directly on the GI tract (duodenum, jejunum, ileum, caecum and colon) by inserting within the lumen through ostomies, for continuous live recordings. A Ag/AgCl wire was inserted in the jejunum lumen as the reference electrode. Recordings of baseline concentrations of serotonin were performed before administration of drugs. Serotonin reuptake inhibitor fluoxetine (10 mg kg^{-1}), monoamine oxidase inhibitor methylene blue (5 mg kg^{-1}) or saline water were administered (1 ml) around the sensing sites by direct injection in the bowel wall. Measurements were performed 10 min after the injection of drugs to the colon tissue. Anaesthetized animals were euthanized by veterinarians at the end of the recordings.

Locomotor and pellet output behaviour. Mice were divided into three groups and behavioural testing was performed by double-blinded individuals. Mice were first anaesthetized in an induction chamber (4% isoflurane) and maintained at 1–2% isoflurane for device implantation. A NeuroString (length 2 cm, width 800 μm, thickness 120 μm) was placed in the colon of one group, flexible Kapton (length 2 cm, width 800 μm, thickness 120 μm) was placed in the colon of the second group and no device was placed in the colon of the third group. After recovering from anaesthesia, mice were placed in a chamber, in which they freely moved. The open-field activity was assessed on the basis of the previously published protocol[56]. The mice were videotaped for 5 min using a Microsoft LifeCam Cinema camera and the movement was analysed using MATLAB.

The pellet output was recorded on the basis of the previously published protocol[57,58]. The same mice were divided into three groups and received NeuroString, flexible Kapton implantation or no implantation into the colon, as described above. After device implantation and recovery from anaesthetization, the mice were placed into a recording chamber. Pellets were collected and counted at the end of the 3-h recording period.

Colitis inflammation model. Colitis was induced by the addition of 2.5% wt./vol. DSS to the drinking water for 10 days (from day 0)[45,59], whereas control mice received normal drinking water. During and after DSS treatment, animals were monitored for signs of pain, altered feeding habits or weight loss to ensure that their nutritional needs are met and there is no notable distress. The colon serotonin was measured in anaesthetized mice by acutely inserting the NeuroString into the mouse colon on different days after the DSS treatment.

Serotonin sensing in living mice. The NeuroString was acutely inserted into the colon to measure the serotonin level in each recording. Mice, fasted overnight, were anaesthetized with 1–2% isoflurane and placed in a stereotaxic apparatus while resting on a heating pad. Following Krebs solution flushing in the colon, the faecal contents in the colon were removed and then lubricant (Medline, E-Z Lubricating Jelly) was placed in the colon with a Teflon tube. The NeuroString probe was inserted into the mouse colon using pullulan as the shuttle material or with the help of an endoscope. Chronoamperometry with a potential of 500 mV was used to monitor the serotonin dynamics. A Ag/AgCl wire was placed in the colon lumen as the reference electrode. The measurements were performed at the distal colon region (2 cm from the anus).

To simultaneously measure the dynamics of brain dopamine and gut serotonin after rewarding consumption, mice with chronically implanted NeuroString (2 months after implantation) in the striatum were used. Mice were first habituated to head fixation, fasted overnight and the NeuroString was inserted into the colon as described above before the sensing experiments. For the reward-intake experiment, 30 μl of chocolate syrup (The Hershey Company) was delivered into the mouth using an oral gavage. The experimenter observed whether the mice consumed the fluid in each session. The brain NeuroString was used to detect the phasic dopamine release in the NAc, whereas the gut NeuroString placed in the colon was used to detect the serotonin concentration over time.

Histology and immunohistology staining. Biocompatibility studies were performed to compare the tissue damages and immune responses at the implantation site for the NeuroString and control devices. To study the brain immune responses, a NeuroString or silica fibre (diameter 100 μm) as control was implanted at the mouse striatum. Three mice (three implants for each mouse) were used for each device. Four weeks after implantation, the mice were euthanized. The brain tissues were fixed in a PBS solution with 4% formaldehyde for 24 h and then in 70% ethanol for 24 h. The sections of tissue samples (thickness 5 μm) were stained with monoclonal antibodies for Iba-1, a microglia marker (Wako Chemicals, 1:400 dilution). and GFAP, an astrocyte marker (Thermo Fisher Scientific 2.2B10, 1:500 dilution). For another batch of mice, the brain sections were cleared and immunostained following a published protocol[60]. Briefly, brain slices (thickness 200 μm) were incubated with CUBIC-L (TCI, T3740) for 48 h and rinsed with PBS. The slices were then incubated with primary antibodies for GFAP (DAKO Z0334, 1:1,000 dilution) and MAP2 (Synaptic Systems 188 004, 1:200) diluted in a staining solution consisting of 0.2% Triton-X and 3% goat serum in PBS for 48 h, and rinsed again in PBS. The slices were then incubated with the secondary antibodies Alexa guinea pig 488 (1:500) and Alexa rabbit 568 (1:500) in the same staining solution for 24 h. After staining, the slices were pretreated with 50% CUBIC-R+ (TCI, T3741) in water for 6 h and then incubated in 100% CUBIC-R+ for 48 h, or until cleared. Imaging was performed using a Leica SP8 confocal microscope.

To study the biocompatibility of devices with the mouse colon, a NeuroString (length 2 cm, width 800 μm, thickness 120 μm) was placed in the colon of one group (three mice). A flexible Kapton film with the same dimensions as the NeuroString was placed in the colon for the control group (three mice). After 3 h, the mice were euthanized by cervical dislocation. The colons were then collected and the longitudinal tissue sections fixed in neutral buffer with 10% formalin (vol./vol.) for 15 h, transferred into 70% ethanol for 5 h and embedded in paraffin. The tissue sections with thickness 5 μm were prepared and stained with H&E staining (completed by the Stanford Department of Comparative Medicine's Animal Histology Services). For the mice treated with DSS, the colons were collected on day 10 after the induction of colitis. The transverse tissue sections (thickness 5 μm) were stained with H&E as well. The stained sections were scanned by a Hamamatsu NanoZoomer 2.0-HT and the images were processed using ImageScope viewing software.

Colonic motility assay. Spatiotemporal mapping was completed according to a published protocol by keeping the caecum on the colon[61]. Twelve-week-old, wild-type male mice were fasted overnight and euthanized by carbon dioxide administration and cervical dislocation. Colons were removed and pinned loosely in the bath containing physiological Krebs solution at 37 °C. A camera (DMK 41AF02, The Imaging Source, Charlotte, NC) was oriented above the tissue and used to record 10-min videos (3.75 fps, 1,280 × 960, 8-bit) using IC Capture software (The Imaging Source, version 2.4.642.2631). Colon samples were randomized to one of three groups to be inserted with different electrodes: (1) a soft NeuroString inserted 2 cm into the distal end; (2) a flexible polyimide inserted 2 cm into the distal end; (3) control group in which no probe was inserted. Custom-written software was used for the analysis of results (VolumetryG9a, Dr. Grant Hennig, University of Vermont). In brief, videos of the colons were transformed into particle formats and a spline was fit longitudinally to measure the diameter over time at every point along the length of the colon. Spatiotemporal maps, which show the matrix of diameter versus time, were generated. From these maps, two thresholds were set to select for long (83 frames, 8–30 s) and short (9 frames, 0.8–3.2 s) intervals between contractions to identify CMMCs and slow-wave-contraction events[62], respectively. A colour gradient was fit to the spatiotemporal maps to represent the interval between slow waves at each cross-sectional diameter for the entire length of the colon. The summation of each focal diameter over the 10-min time period was normalized to graph the cumulative distribution of the percentile of intervals (in seconds) of CMMCs and slow-wave contractions. The method and source code for the ex vivo gut segment diameter mapping recipe is provided in the Supplementary Information.

Statistical analysis

For statistical analyses, R, Origin, Prism and Excel were used. All replicate numbers, error bars, *P*-values and statistical tests are indicated in the figure legends.

Reporting summary

Further information on research design is available in the Nature Research Reporting Summary linked to this paper.

Data availability

The datasets generated during and/or analysed in this study are available from the corresponding author on reasonable request. The method and source code for the ex vivo gut segment diameter mapping recipe is provided in the Supplementary Information. Source data are provided with this paper.

48. Singh, M. K. & Bandyopadhyay, D. Design and synthesis of nanoporous perylene bis-imide linked metalloporphyrin frameworks and their catalytic activity. *J. Chem. Sci.* **128**, 1–8 (2016).
49. Lin, J. et al. Laser-induced porous graphene films from commercial polymers. *Nat. Commun.* **5**, 5714 (2014).
50. Metscher, B. D. MicroCT for comparative morphology: Simple staining methods allow high-contrast 3D imaging of diverse non-mineralized animal tissues. *BMC Physiology* **9**, 11 (2009).
51. Roberts, J. G. & Sombers, L. A. Fast-scan cyclic voltammetry: chemical sensing in the brain and beyond. *Anal. Chem.* **90**, 490–504 (2018).
52. Howard, C. D., Li, H., Geddes, C. E. & Jin, X. Dynamic nigrostriatal dopamine biases action selection. *Neuron* **93**, 1436–1450.e8 (2017).
53. Stamford, J. A., Kruk, Z. L. & Millar, J. Striatal dopamine terminals release serotonin after 5-HTP pretreatment: in vivo voltammetric data. *Brain Res.* **515**, 173–180 (1990).
54. Swamy, B. E. K. & Venton, B. J. Carbon nanotube-modified microelectrodes for simultaneous detection of dopamine and serotonin in vivo. *Analyst* **132**, 876–884 (2007).
55. Jackson, B. P. & Mark Wightman, R. Dynamics of 5-hydroxytryptamine released from dopamine neurons in the caudate putamen of the rat. *Brain Res.* **674**, 163–166 (1995).
56. Tatem, K. S. et al. Behavioral and locomotor measurements using an open field activity monitoring system for skeletal muscle diseases. *J. Vis. Exp.* **29**, 51785 (2014).
57. Lynch, J. J., Castagné, V., Moser, P. C. & Mittelstadt, S. W. Comparison of methods for the assessment of locomotor activity in rodent safety pharmacology studies. *J. Pharmacol. Toxicol. Methods* **64**, 74–80 (2011).
58. Hoibian, E., Florens, N., Koppe, L., Vidal, H. & Soulage, C. O. Distal colon motor dysfunction in mice with chronic kidney disease: putative role of uremic toxins. *Toxins* **10**, 204 (2018).
59. Wirtz, S. et al. Chemically induced mouse models of acute and chronic intestinal inflammation. *Nat. Protoc.* **12**, 1295–1309 (2017).
60. Tainaka, K. et al. Chemical landscape for tissue clearing based on hydrophilic reagents. *Cell Rep.* **24**, 2196–2210.e9 (2018).
61. Swaminathan, M. et al. Video imaging and spatiotemporal maps to analyze gastrointestinal motility in mice. *J. Vis. Exp.* **2016**, e53828 (2016).
62. Spear, E. T. et al. Altered gastrointestinal motility involving autoantibodies in the experimental autoimmune encephalomyelitis model of multiple sclerosis. *Neurogastroenterol. Motil.* **30**, e13349 (2018).

Acknowledgements This work was partly supported by the Stanford Bio-X Interdisciplinary Initiatives Seed Grants Program (IIP award) and the Wu Tsai Neuroscience Institute Big Idea Award. Part of this work was performed at the Stanford Nano Shared Facilities (SNSF), supported by the National Science Foundation under award ECCS-1542152. X.C. and L.Y. are partially supported by National Institutes of Health grants R01DA045664, R01MH116904 and R01HL150566, and X.C. is also supported by the Firmenich Next Generation Fund. Y.L. is supported by National Science Scholarship (A*STAR, Singapore). Part of the electrochemical measurement experiments during revision was conducted at Michigan State University. We thank N. G. Hollon and X. Jin from the Salk Institute for their help with the FSCV technique; G. Hennig (University of Vermont) for the design and use of Volumetry software; S. Baker and A. Zhang for their help on pig animal surgery; S. Das from the Julia Kaltschmidt lab for the help on the colonic motility assay setup; S. Rogalla for the endoscope imaging; T. Z. Gao for comments on the manuscript; and Y. Tsao, S. Chen and Y. Liu for their help on materials characterization.

Author contributions J.L., Y.L., X.C. and Z.B. conceived the project. J.L., Y.L., L.Y., X.C., Z.B., E.S.B. and A.H. designed the experiments. J.L. and Y.L. designed and fabricated the device and performed the mechanical, electrical and electrochemical measurements. K.W. synthesized the metalloporphyrin. J.L., Y.L. and Y.-Q.Z. performed the SEM, CT and photography. J.T. and G.C. performed the EELS, HRTEM, SEM and Raman characterizations. J.L., Y.L., L.Y., B.Z. and E.S.B. carried out the ex vivo experiments and animal studies. S.N. and L.B. contributed to the initial materials selection. M.D., A.-L.T. and J.C.Y.D. developed the pig animal model and protocol. W.X. helped to prepare the schematics. V.M. helped to analyse the voltammograms. T.L.L., B.C. and S.P.P. contributed to characterization of tissue responses. J.L., Y.L. and E.S.B. analysed the results. J.L., Y.L., X.C., Z.B. and J.B.-H.T. wrote the manuscript. All authors discussed the results and commented on the manuscript. All authors have given approval to the final version of the manuscript. Z.B. and X.C. directed the project.

Competing interests J.L., Y.L. and Z.B. are inventors on a patent application (no. 63/085,720) submitted by the Board of Trustees of Stanford University.

Additional information

Supplementary information The online version contains supplementary material available at https://doi.org/10.1038/s41586-022-04615-2.

Correspondence and requests for materials should be addressed to Xiaoke Chen or Zhenan Bao.

Peer review information *Nature* thanks Giovanni Traverso and the other, anonymous, reviewers for their contribution to the peer review of this work.

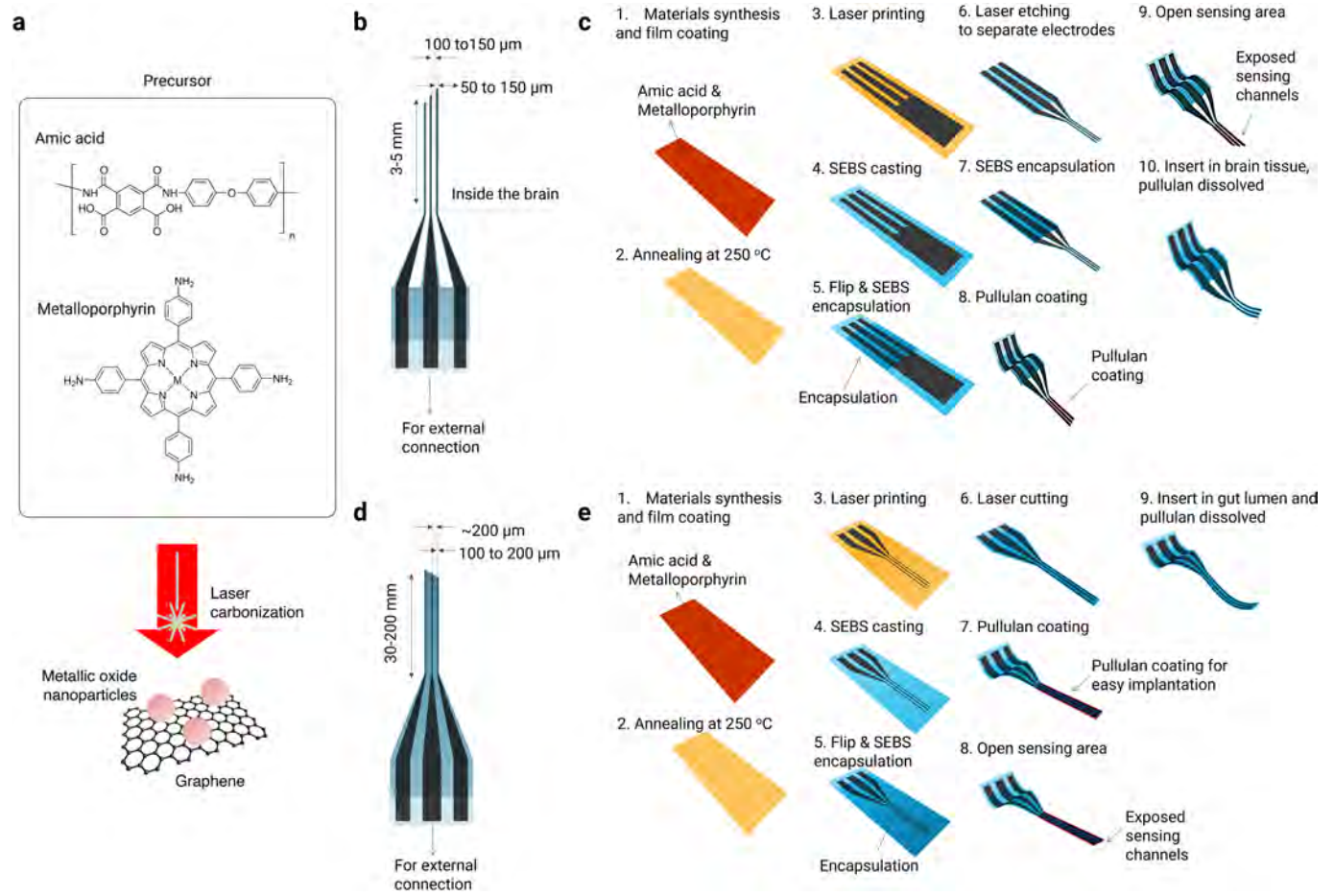

Extended Data Fig. 1 | Fabrication process of the NeuroString sensors. **a**, Scheme showing the chemical structures of the polymer precursors and the laser carbonization process. **b**, Layout showing the dimensions of the multichannel NeuroString electrodes for the sensing in the brain. **c**, Fabrication process of the NeuroString for brain neurochemical sensing. (1) A polymer precursor solution containing a polyamic acid mixed with a metalloporphyrin (2.3×10^{-1} mM) was uniformly drop-casted (50 μl cm^{-2}) as a film on a polyimide substrate. (2) The precursor film was annealed in air at 250 °C for 1 h to form the polyimide film. (3) The film surface was laser engraved by an Epilog Fusion M2 laser (power 6 W) to generate the graphene network with Fe_3O_4 or NiO nanoparticles. A HPDFO lens with a focal point of 0.001″ (25.4 μm) can be used improve the resolution of the engraving. (4) A SEBS solution (H1062, 0.1 g ml^{-1} in toluene) was drop-casted on the graphene networks, which was then peeled off from the substrate and attached to another glass substrate when the SEBS side was in contact with glass. (5) Another SEBS layer (H1062, 0.1 g ml^{-1} in toluene) was spin-coated on top at 1,000 rpm, to form an encapsulation layer. (6) A high laser power of 30 W was subsequently used to cut into the desired size and shape and isolate the individual electrode strings with width 90 μm. (7) The electrode area is dip-coated in another elastomer solution (Kuraray LA3320, 0.1 g ml^{-1} in acetone) to fully encapsulate the graphene electrodes. (8) For implantation in the brain, the NeuroStrings were dip-coated in a pullulan solution (0.3 g ml^{-1}) and dried overnight to form a rigid coating. (9) The tips of electrodes were cut by a razor blade to expose the cross sections of the graphene. To fully expose the graphene, the cross-sectional surfaces of electrodes were oxygen plasma-treated for 2 min (Technics Micro-RIE Series 800, 150 W, 200 mTorr). To avoid any electrochemical interference of the ascorbic acid from the biological fluids, the tips of the electrodes were dipped in a Nafion solution (0.5% in water/ethanol) to form a Nafion coating before use. (10) Dissolving of the pullulan in tissue finally releases the NeuroString as a soft implant. **d**, Layout showing the dimensions of the NeuroString electrodes for sensing in the gut. **e**, Fabrication process of the NeuroString for gut neurochemical sensing. (1) A polymer precursor solution containing a polyamic acid mixed with a metalloporphyrin (2.3×10^{-1} mM) was uniformly drop-casted (50 μl cm^{-2}) as a film on a polyimide substrate. (2) The precursor film was annealed in air at 250 °C for 1 h to form the polyimide film. (3) The film surface was laser engraved by an Epilog Fusion M2 Laser (power 6 W) to generate the graphene network with Fe_3O_4 or NiO nanoparticles. (4) SEBS solution (H1062, 0.1 g ml^{-1} in toluene) was drop casted on the graphene networks to form graphene–SEBS composite, which was then delaminated and transferred from the substrate and flipped on another glass substrate. (5) Another SEBS layer (H1062, 0.1 g ml^{-1} in toluene) was spin-coated on top at 1,000 rpm, to form an encapsulation layer. (6) A high-power laser with power 30 W and 20% speed was used to cut the undesired part of the device. (7) For easier placing the mouse gut, a pullulan solution (0.1 g ml^{-1}) was dip-coated on the electrodes and dried overnight to form the shuttle layer. (8) The ends of electrodes were cut using a razor blade to expose the cross sections of the graphene. To fully expose the graphene, the cross-sectional surfaces of electrodes were oxygen plasma-treated for 2 min. To avoid any interference of the ascorbic acid from the biological fluids, the tips of the electrodes were finally dipped in a Nafion solution (0.5% in water/ethanol) to form a Nafion coating before use. (9) Dissolving of the pullulan in tissue will release the NeuroString as a soft implant.

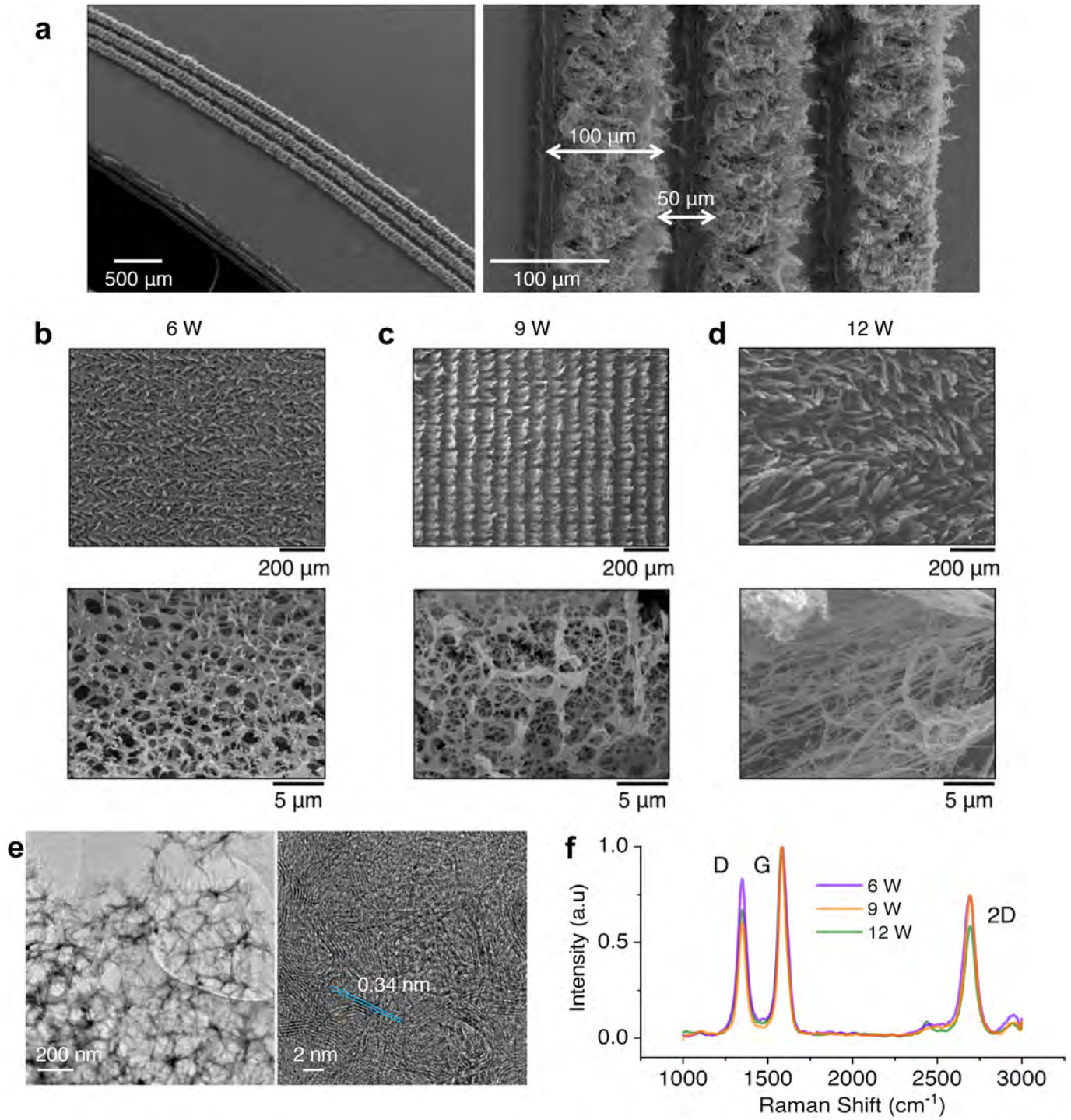

Extended Data Fig. 2 | Characterization of the laser-induced graphene used in the NeuroString sensor. a, SEM images showing the resolution of the laser fabrication process (laser power 6 W). Direct laser writing can achieve a resolution of about 100 µm, whereas individual structures smaller than 50 µm can be fabricated by the laser engraving (etching) process: for example, two laser cutting lines with a distance of 150 µm will lead to a free-standing electrode of width 50 µm. **b**–**d**, SEM images showing the graphene networks made by different laser powers. The graphene layer thicknesses are: 40–50 µm (laser power 6 W), 50–80 µm (laser power 9 W) and 120–150 µm (laser power 12 W). Thicker polyimide film will be carbonized at a higher laser power, so that the graphene layer increases. The SEM characterization was repeated and reproduced six times. **e**, High-resolution TEM of laser-induced graphene showing the characteristic 0.34-nm *d*-spacing between graphene sheets (laser power 6 W). The TEM characterization was repeated and reproduced three times. **f**, Normalized confocal Raman spectra (633-nm laser excitation) of a laser-induced graphene film made by different laser powers. The intensity profile indicates that higher laser power induced more defects in graphene. The higher D band at lower laser power is mainly owing to the more oxygen and graphene oxide present in the laser-induced graphene.

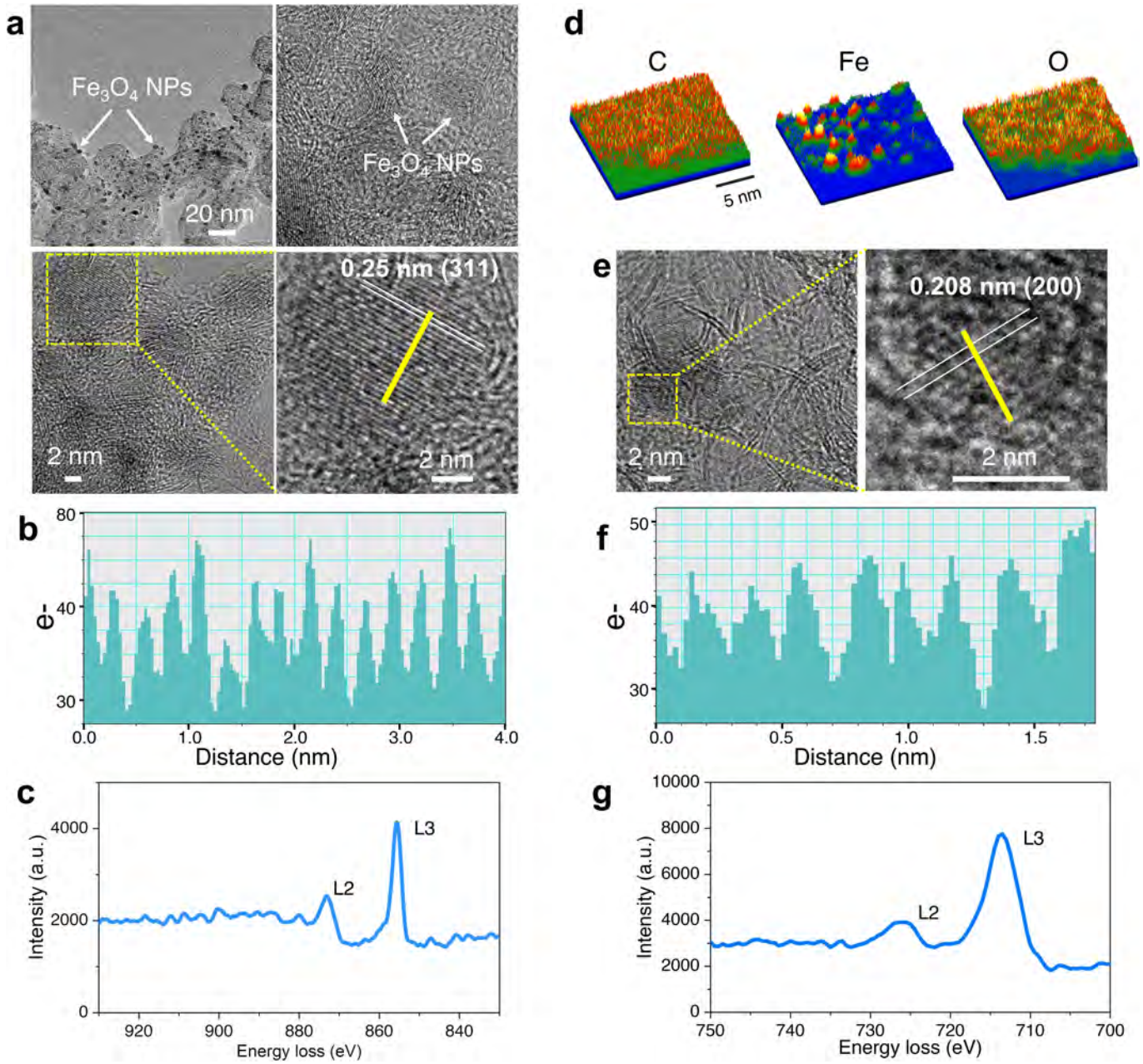

Extended Data Fig. 3 | Characterization of the transition metal oxide nanoparticles involved in the NeuroString sensor. a, TEM characterization of the laser-induced graphene decorated with Fe_3O_4 nanoparticles (laser power 6 W). The TEM characterization was repeated and reproduced three times. **b**, TEM intensity profile of the Fe_3O_4 nanocrystal shown in **a**. **c**, EELS analysis of the laser-induced graphene decorated with Fe_3O_4 nanoparticles (laser power 6 W). **d**, EELS mapping showing decoration of Fe_3O_4 nanoparticles on the graphene. **e**, TEM characterization of the laser-induced graphene decorated with NiO nanoparticles (laser power 6 W). The TEM characterization was repeated and reproduced three times. **f**, TEM intensity profile of the NiO nanocrystal shown in **e**. **g**, EELS analysis of the laser-induced graphene decorated with NiO nanoparticles (laser power 6 W).

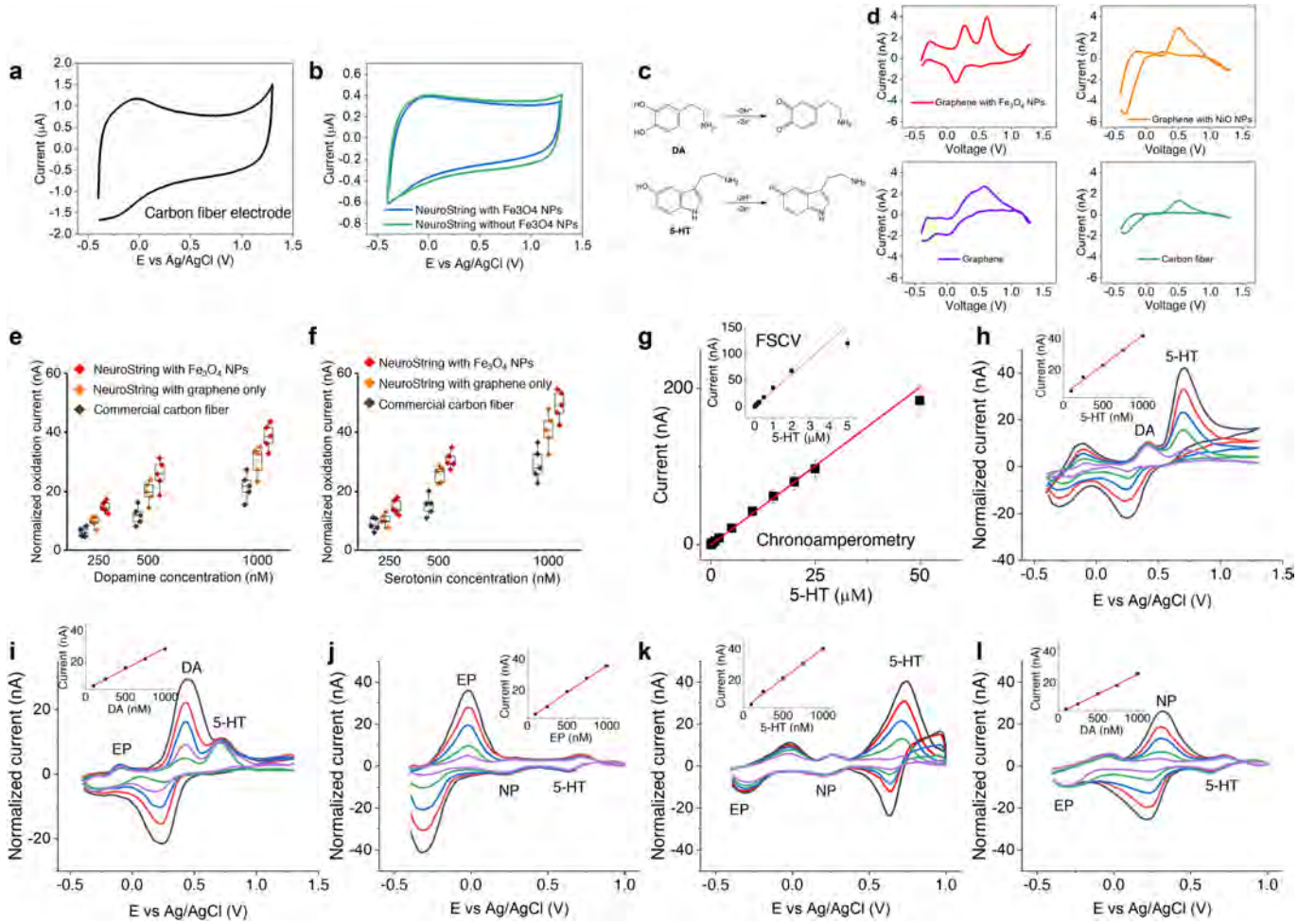

Extended Data Fig. 4 | Selectivity and sensitivity characterization of the NeuroString sensors. a, **b**, Cyclic voltammetry backgrounds of different electrodes in PBS buffer (pH 7.4) (scan rate 400 V s^{-1}). NeuroString has lower background current than the carbon fibre. **c**, Reaction mechanism of the dopamine and serotonin oxidation during FSCV measurement. **d**, Comparison of the selectivity of different electrodes for simultaneous dopamine and serotonin sensing using cyclic voltammetry. The cyclic voltammetry is performed in a solution with 500 nM dopamine and 500 nM serotonin in PBS (pH 7.4), with a scan rate of 10 V s^{-1}. **e**, **f**, Normalized oxidation current (nA) of NeuroString (without and with Fe_3O_4 nanoparticles) and carbon nanofibres for dopamine and serotonin sensing (scan rate 400 V s^{-1}). As the background current varies from 100 to 500 nA depending on the dimension, the normalized oxidation current = $\frac{\text{Background current}}{\text{Faradic current}} \times 1,000$ nA; the background current is defined as the current value at 0.5 V. $n = 5$ different NeuroString electrodes were examined in independent measurements, box range: 25–75%. **g**, Concentration-dependent calibration response of NeuroString electrode to 5-HT using FSCV and chronoamperometry. (PBS buffer pH 7.4; chronoamperometry potential: 0.6 V, error bars are obtained from $n = 6$ different NeuroString electrodes examined in independent measurements.) Simultaneous and selective detection of DA and 5-HT. **h**, FSCV of various concentrations of 5-HT (100 nM, 250 nM, 500 nM, 750 nM, 1,000 nM) in 200 nM DA solution (dissolved in PBS buffer, pH 7.4); inset shows the linear plot of currents against concentrations of 5-HT. **i**, FSCV of various concentrations of DA (100 nM, 250 nM, 500 nM, 750 nM, 1,000 nM) in 200 nM 5-HT solution (dissolved in PBS buffer, pH 7.4); inset shows the linear plot of currents against concentrations of DA. Simultaneous and selective detection of NP, EP and 5-HT. **j**, FSCV of various concentrations of EP (100 nM, 250 nM, 500 nM, 750 nM, 1,000 nM) in 200 nM 5-HT and 200 nM EP solution (dissolved in PBS buffer, pH 7.4); inset shows the linear plot of currents against concentrations of EP. **k**, FSCV of various concentrations of 5-HT (100 nM, 250 nM, 500 nM, 750 nM, 1,000 nM) in 200 nM NP and 200 nM EP solution (dissolved in PBS buffer, pH 7.4); inset shows the linear plot of currents against concentrations of 5-HT. **l**, FSCV of various concentrations of NP (100 nM, 250 nM, 500 nM, 750 nM, 1,000 nM) in 200 nM 5-HT and 200 nM EP solution (dissolved in PBS buffer, pH 7.4); inset shows the linear plot of currents against concentrations of NP.

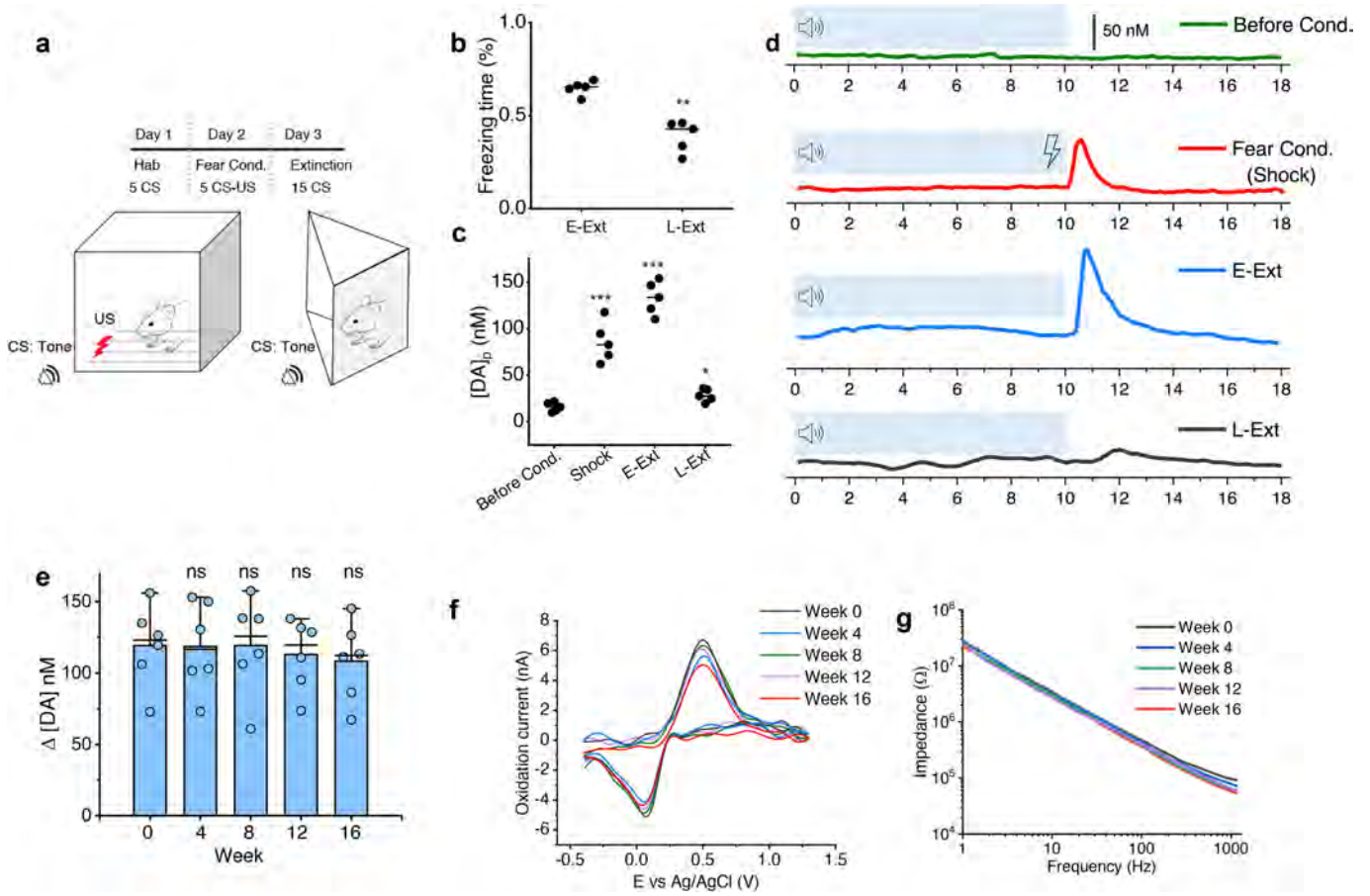

Extended Data Fig. 5 | Measurement of the neurotransmitter release during fear conditioning and extinction training, and chronic stability of the NeuroString for neurotransmitter sensing. a–**d**, Dopamine release in the NAc measured during various phases of a fear extinction task (NeuroStrings were implanted at least two weeks before the behaviour assay started). **a**, Trial structure for the fear extinction training. **b**, Percentage of freezing to the CS during the early extinction phase (E-Ext, 1–8 trials) and the late extinction phase (L-Ext, 9–15 trials) ($n = 5$ mice). The CS evoking lower freezing levels during the late phase indicated successful extinction learning. *P*-value 0.0005. **c**, Quantification of dopamine responses to the CS during habituation (before Cond.), the fear conditioning (an electric shock after the tone) and fear extinction phase ($n = 5$ mice). *P*-values: 0.0018 (shock), 0.003 (E-Ext), 0.0706 (L-Ext). **d**, Exemplar time-aligned dopamine signals from a mouse during each phase. **e**, Chronic measurement of dopamine in the NAc evoked by optogenetic stimulation of dopamine neurons in the VTA of DAT-Cre mice expressing ChR2 (error bars are obtained from measurements from $n = 6$ biologically independent mice). *P*-values: 0.9011 (week 4), 0.9926 (week 8), 0.6946 (week 12), 0.4462 (week 16). **f**, **g**, Representative measurements from a NeuroString electrode in a mouse across 16 weeks in the form of background-subtracted cyclic voltammogram (**f**) and the corresponding electrochemical impedance (**g**). *P*-values are calculated by paired two-tailed Student's *t*-test: NS, $P > 0.05$; $^{*}P \leq 0.05$; $^{**}P \leq 0.01$; $^{***}P \leq 0.001$.

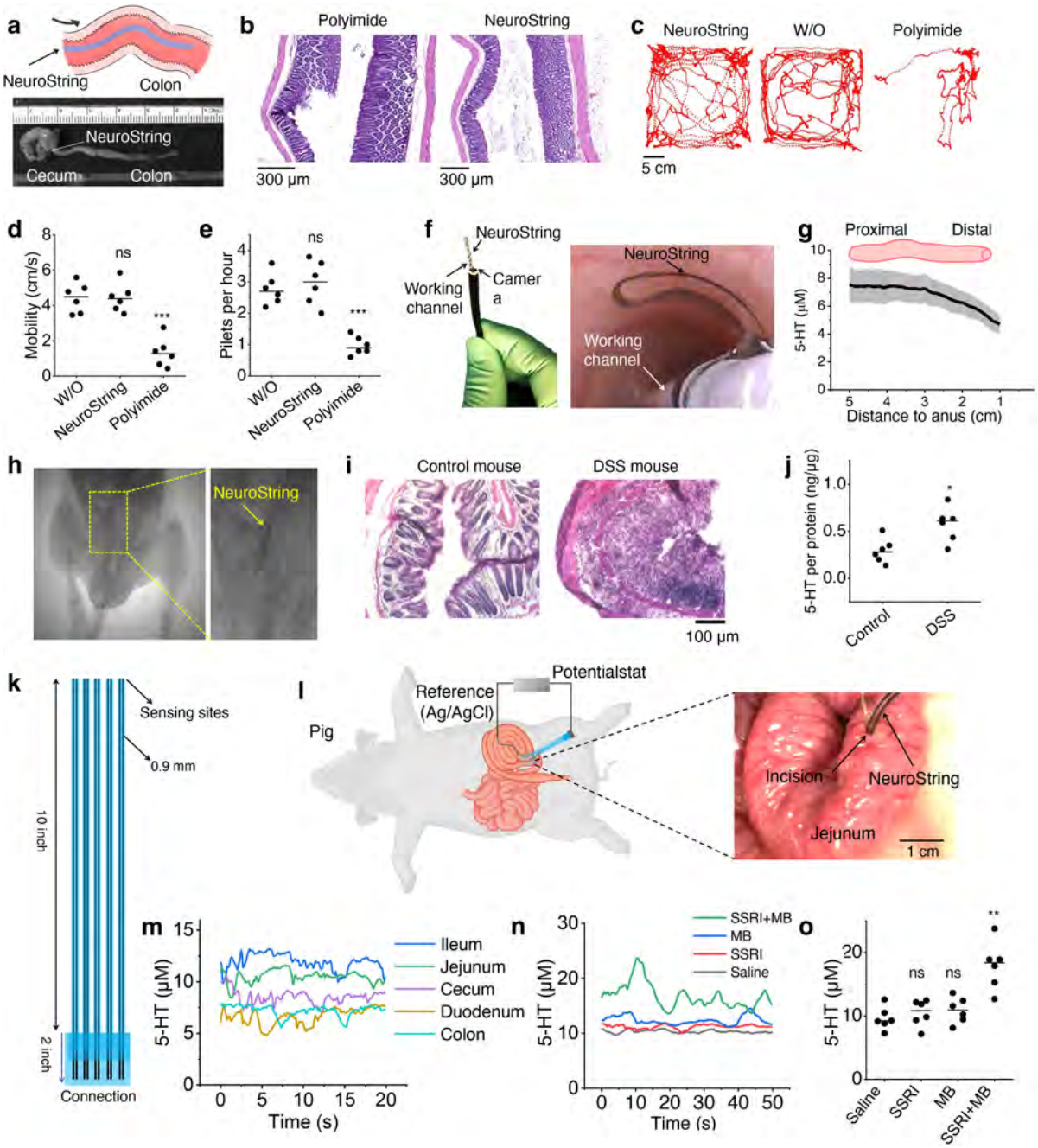

Extended Data Fig. 6 | See next page for caption.

Extended Data Fig. 6 | Evaluation of NeuroString performance for serotonin sensing in the GI tract of rodents and large animals. a, Setup of the colonic motility assay providing video imaging and spatiotemporal maps to analyse colonic motility of mice inserted with NeuroString ex vivo. Control is a mouse colon without anything inside the lumen. **b**, Representative H&E staining images showing the colon tissue of mice placed with a flexible Kapton (length 2 cm, width 800 μm, thickness 120 μm) film and a NeuroString with the same dimensions. The materials were placed in the colon of freely moving mice for 3 h before collecting the tissue. Damage to the tissue was clearly observed with flexible polyimide film implant. The H&E staining was repeated and reproduced for five mice. Open-field activity (average velocity) (**c**, **d**) and pellet output (**e**) over a 5-h period for mice with the colon acutely placed with a NeuroString or a flexible Kapton polyimide as control ($n = 6$). *P*-values: NeuroString (0.9689), polyimide (0.0004) in **d**; NeuroString (0.4895), polyimide (0.0015) in **e**. The dotted lines in **c** show 5-min trajectories of the mice. **f**, Photos showing NeuroString wrapped around a probe extended from one working channel of an endoscope (left) and the obtained endoscopy photo showing the NeuroString entering the colon lumen for serotonin sensing in a rat model (right). **g**, Representative serotonin concentration mapping in the rat colon (5 cm from the anus) collected by delivering the NeuroString into the colon lumen and slowly taking it out (error bar denotes ±standard deviation of the measurement results obtained from three channels). **h**, μ-CT images showing the NeuroString conformally loaded in the mouse colon. **i**, Representative H&E staining images showing the colon tissue of control mouse treated with saline water and colitis mouse with inflammation induced by DSS after 10 days of colitis development. The H&E staining was repeated and reproduced for five mice. **j**, Measured serotonin concentration in the colon tissue of control and DSS mice using enzyme-linked immunosorbent assay. *P*-value 0.0171. **k**, Layout of the NeuroString sensor for serotonin sensing in the pig colon. The sensor fabrication process is the same as that illustrated in Extended Data Fig. 1, except for the use of a large polyimide sheet (12″ × 12″) as a substrate. **l**, Scheme and photo showing the multiple-site serotonin measurement in the intestine of a pig by NeuroString. **m**, Simultaneous serotonin sensing in different segments of the intestinal tract by multiple-channel NeuroString. **n**, **o**, Drug-induced luminal serotonin concentration change using fluoxetine (SSRI), MB, fluoxetine (SSRI) + MB and saline as control ($n = 6$ pigs). *P*-values: SSRI (0.5553), MB (0.3567), SSRI + MB (0.0099). *P*-values are calculated by paired two-tailed Student's *t*-test: NS, $P > 0.05$; $^{*}P \leq 0.05$; $^{**}P \leq 0.01$; $^{***}P \leq 0.001$.

nature portfolio

Corresponding author(s): Zhenan Bao, Xiaoke Chen

Last updated by author(s): Feb 11, 2022

Reporting Summary

Nature Portfolio wishes to improve the reproducibility of the work that we publish. This form provides structure for consistency and transparency in reporting. For further information on Nature Portfolio policies, see our Editorial Policies and the Editorial Policy Checklist.

Statistics

For all statistical analyses, confirm that the following items are present in the figure legend, table legend, main text, or Methods section.

n/a	Confirmed
☐	☒ The exact sample size (*n*) for each experimental group/condition, given as a discrete number and unit of measurement
☐	☒ A statement on whether measurements were taken from distinct samples or whether the same sample was measured repeatedly
☐	☒ The statistical test(s) used AND whether they are one- or two-sided *Only common tests should be described solely by name; describe more complex techniques in the Methods section.*
☒	☐ A description of all covariates tested
☒	☐ A description of any assumptions or corrections, such as tests of normality and adjustment for multiple comparisons
☐	☒ A full description of the statistical parameters including central tendency (e.g. means) or other basic estimates (e.g. regression coefficient) AND variation (e.g. standard deviation) or associated estimates of uncertainty (e.g. confidence intervals)
☐	☒ For null hypothesis testing, the test statistic (e.g. *F*, *t*, *r*) with confidence intervals, effect sizes, degrees of freedom and *P* value noted *Give P values as exact values whenever suitable.*
☒	☐ For Bayesian analysis, information on the choice of priors and Markov chain Monte Carlo settings
☒	☐ For hierarchical and complex designs, identification of the appropriate level for tests and full reporting of outcomes
☒	☐ Estimates of effect sizes (e.g. Cohen's *d*, Pearson's *r*), indicating how they were calculated

Our web collection on statistics for biologists contains articles on many of the points above.

Software and code

Policy information about availability of computer code

Data collection	Electrochemical-impedance and cyclic-voltammetry data were collected with Palmsens PSTrace5; mechanical tests were collected with Bluehill 3 Testing Software. The mice colonic motility video analysis was performed using custom-written software (VolumetryG9a, Dr. Grant Hennig, University of Vermont).
Data analysis	Electrochemical-impedance and cyclic-voltammetry data were analysed by using Palmsens PSTrace5 , Microsoft Excel 2016 (version 1807,10325.20082), and OriginPro 2016 b9.3.226 (64-bit) . Mechanical test data were analysed by using OriginPro 2016 b9.3.226 (64-bit) and Microsoft Excel 2016 (version 1807, 10325.20082). Immunofluorescence data were analysed by using ImageJ bundled with 64-bit Java 1.8.0_172, Aperio ImageScope 12.4.3, OriginPro 2016 b9.3.226 (64-bit) and Microsoft Excel 2016 (version 1807,10325.20082). P value was calculated by software Prism and R. The projection X-ray images were reconstructed into 3D images and processed using software Dragonfly (Object Research System).

For manuscripts utilizing custom algorithms or software that are central to the research but not yet described in published literature, software must be made available to editors and reviewers. We strongly encourage code deposition in a community repository (e.g. GitHub). See the Nature Portfolio guidelines for submitting code & software for further information.

Data

Policy information about availability of data

All manuscripts must include a data availability statement. This statement should provide the following information, where applicable:

- Accession codes, unique identifiers, or web links for publicly available datasets
- A description of any restrictions on data availability
- For clinical datasets or third party data, please ensure that the statement adheres to our policy

The authors declare that all data supporting the findings of this study are available within the paper and its Supplementary Information.

Field-specific reporting

Please select the one below that is the best fit for your research. If you are not sure, read the appropriate sections before making your selection.

☒ Life sciences ☐ Behavioural & social sciences ☐ Ecological, evolutionary & environmental sciences

For a reference copy of the document with all sections, see nature.com/documents/nr-reporting-summary-flat.pdf

Life sciences study design

All studies must disclose on these points even when the disclosure is negative.

Sample size	Sample size was not calculated beforehand. Sample size was determined by the number of biological and technical replicates necessary to convince us that the effect was real. The number of biological replicates we aimed for was 4-6, with several technical replicates in each sample.
Data exclusions	No data were excluded from the analyses.
Replication	All experimental findings, including ex vivo measurements, living animal measurements, SEM images, TEM images, microCT, electrochemical characterization, mechanical characterization, and electrical characterization were reliably reproduced for 3-6 times.
Randomization	Experimental groups were allocated by random selections.
Blinding	Ex vivo study and living animal study were divided into matched groups and behavior testing was performed by double-blinded individuals.

Reporting for specific materials, systems and methods

We require information from authors about some types of materials, experimental systems and methods used in many studies. Here, indicate whether each material, system or method listed is relevant to your study. If you are not sure if a list item applies to your research, read the appropriate section before selecting a response.

Materials & experimental systems

n/a	Involved in the study
☐	☒ Antibodies
☒	☐ Eukaryotic cell lines
☒	☐ Palaeontology and archaeology
☐	☒ Animals and other organisms
☒	☐ Human research participants
☒	☐ Clinical data
☒	☐ Dual use research of concern

Methods

n/a	Involved in the study
☒	☐ ChIP-seq
☒	☐ Flow cytometry
☒	☐ MRI-based neuroimaging

Antibodies

Antibodies used	Primary antibodies used in this work include antibodies for GFAP (DAKO Z0334, at a 1:1000 dilution or Thermo Fisher Scientific 2.2B10, 1:500 dilution) and MAP2 (Synaptic Systems 188004, at a 1:200 dilution), Iba-1 (Wako Chemicals, 1:400 dilution); Secondary antibodies used in this work include Alexa guinea pig 488 (1:500) and Alexa rabbit 568 (1:500), Goat AntiRabbit IgG H&L (Alexa Fluor® 488) (Abcam ab150077), Goat Anti-Mouse IgG H&L (Alexa Fluor® 647) (Abcam ab150115).
Validation	Validation of each antibody was done under standard information offered by the supplier.

Animals and other organisms

Policy information about studies involving animals; ARRIVE guidelines recommended for reporting animal research

Laboratory animals	Wild-type C57Bl/6J male mice; DAT-Cre mice with viral expression of ChR2 (The Jackson Laoratory, No: 006660); Sert-Cre mice with viral expression of ChR2 (The Jackson Laoratory, No: 014554); All wild-type C57BL/6J, DAT-Cre and Sert-Cre mice used in this study were 8–12-week-old males. The DAT-Cre (No: 006660) and Sert-Cre (No: 014554) mice were initially purchased from Jackson Laboratory and bred in the facility. The housing facility is maintained at ~22°C and 35%–55% humidity on a 12-h light/dark cycle (lights on at 7:00 am). Female juvenile mini-Yucatan pigs (age 6-9 weeks, and weight of 10 kg, from breeder S&S Farms, Ramona, CA), Housed in pathogen-free rooms with alternate light/dark cycle, fed with liquid diet; Male Sprague Dawley rats (50–150 g, Charles River). The housing facility is maintained at ~22°C and 35%–55% humidity on a 12-h light/dark cycle (lights on at 7:00 am).
Wild animals	The study did not involve wild animals
Field-collected samples	The study did not involve field-collected samples
Ethics oversight	All procedures involving implantation and harvesting of electrodes on rat sciatic nerves were performed in accordance with protocols approved by the Institutional Animal Care and Use Committee (IACUC) at the Stanford University.

Note that full information on the approval of the study protocol must also be provided in the manuscript.